Modeling Composite Laminate Crushing for Crash Analysis

Summary of Research
5/15/2000–12/15/2001

David C. Fleming
Assistant Professor
Aerospace Engineering
Florida Institute of Technology
150 W. University Blvd.
Melbourne, FL 32901
dfleming@fit.edu

NAG-1-2260

INTRODUCTION

Crash modeling of composite structures remains limited in application and has not been effectively demonstrated as a predictive tool. While the global response of composite structures may be well modeled, when composite structures act as energy-absorbing members through direct laminate crushing the modeling accuracy is greatly reduced. The most efficient composite energy absorbing structures, in terms of energy absorbed per unit mass, are those that absorb energy through a complex progressive crushing response in which fiber and matrix fractures on a small scale dominate the behavior [1,2]. Such failure modes simultaneously include delamination of plies, failure of the matrix to produce fiber bundles, and subsequent failure of fiber bundles either in bending or in shear. In addition, the response may include the significant action of friction, both internally (between delaminated plies or fiber bundles) or externally (between the laminate and the crushing surface). Figure 1 shows the crushing damage observed in a fiberglass composite tube specimen, illustrating the complexity of the response. To achieve a finite element model of such complex behavior is an extremely challenging problem. A practical crushing model based on detailed modeling of the physical mechanisms of crushing behavior is not expected in the foreseeable future. The present research describes attempts to model composite crushing behavior using a novel hybrid modeling procedure. Experimental testing is done is support of the modeling efforts, and a test specimen is developed to provide data for validating laminate crushing models.

PREVIOUS RESEARCH

Several researchers have attempted finite element models of composite crushing behavior, with varying degrees of success. The modeling approaches followed by previous researchers are categorized by approach, and include models based on in-plane failure and damage mechanics, as well as modeling efforts that attempt to model the crushing phenomenology in greater detail, and hybrid modeling approaches that model crushing response via simplified empirical models. Efforts in each of these areas are reviewed below[1].

In-Plane Failure and Damage Mechanics

For efficient modeling, composite structures are often represented by shell elements. The properties of the shell elements allow for arbitrary composite lay-ups and may allow failure and property degradation of each individual ply to be predicted using either conventional in-plane failure predictions or other damage mechanics models. Because such failure models do not typically allow treatment of out-of-plane failures, particularly delamination, the general crushing behavior of composites cannot be modeled. Such approaches are therefore more likely to be effective for material and structural configurations that result in failure modes such as local buckling, or are dominated by global effects such as tearing of a wall, than for failure modes that result in wholesale destruction of the material. As a result, the success of these approaches is more likely for material/structural configurations that have suboptimal energy absorbing performance. Some of the efforts reported in the literature for modeling composite crushing using these methods are reviewed in the following paragraphs.

[1] The following sections are largely derived from a conference paper entitled "Modeling Delamination Growth in Composites using MSC.Dytran" presented by the author at the 2nd *Worldwide Automotive Conference*, Oct. 9-11, 2000, Dearborne, MI [3].

Haug et al. [4] describe a composites damaging model implemented in PAM-CRASH. This model treats the fiber and matrix in a filamentary composite as distinct phases from which the overall properties of the ply are derived. Damage parameters are introduced for the fiber and matrix phases. The values of these parameters are determined based on volumetric and deviatoric strain components in each of the phases. Elastic properties of the phases are reduced according to the calculated damage parameters. Reference 4 describes some initial investigations using this method to predict the crushing of composite tube structures, such as might be used in automotive applications. The model appears to be successful for modeling columns that fail in a local buckling failure mode or by progressive folding from one of the ends. For a structure with a more brittle failure mechanism, the results appear less encouraging. Other researchers have used and advanced this method. Kermanidis et al [5] used this approach to model the crushing of a sinewave beam element. Comparison with experimental results is not clear, but the crushing load appears to have been underpredicted. Kohlgrüber and Kamoulakos [6] used the PAM-CRASH bi-phase model, enhanced to handle fabric composites, to model the crushing of carbon/Kevlar hybrid composite tube segments (roughly semicircular) as well as simulated elements of helicopter subfloor structures. For the tube segment models, it was noted that behavior such as delamination in the crashfront could not be modeled, and a more detailed model using solid elements and breakable constraints at ply interfaces was attempted to produce better results. For the larger structural models, a reasonable agreement between finite element and experimental results is shown. However, photographs of the deformed specimens show that failure is dominated by large-scale failures such as tearing at structural intersections and buckling of walls, and that relatively little wholesale crushing behavior is evident. Johnson and his collaborators [7,8] show additional models based on this approach.

Other damage mechanics models have been proposed. Faruque and Wang [9] present a model in which elastic properties of a ply are degraded by two damage parameters controlled by tensile strains in the shell element. The properties are related to the fiber principle directions, and do not utilize a micromechanics approach as in the bi-phase model above. A modification of the model to account for inelastic behavior typical of braided composites is also shown. Results for a braided glass/vinylester tube are shown and compared with experimental results. Lee and Simunovic [10] present a constitutive model for random fiber composites based on an elastoplastic model. Progressive fiber/matrix debonding is predicted based on a statistical model. The model is implemented in DYNA3D, and demonstrated for a problem involving the crushing of a square tube. Failure is dominated by tearing of the composites at the corners. Tabei and Chen [11] present a micromechanical model for composites. Various failure criteria are applied to predict behaviors such as fiber fracture, matrix cracking, and fiber microbuckling. A model of a square graphite/epoxy tube is shown, but no comparison with experimental results is made. The failure mode in the finite element model appears to be a folding mode.

A different approach from the damaging models described above, based on classical laminated plate theory, is presented by Matzenmiller and Schweizerhof [12]. This material model, called the enhanced composite damaging model, is implemented in LS-DYNA as material types 54/55, [12] and the subsequently refined composite damaging material types 58/59 [13]. The model allows for conventional failure of plies predicted based on ply stresses and conventional strength properties. However, a "crashfront" procedure is added to address the crushing response of

composite structures, albeit in an empirical fashion. An erosion feature is used to eliminate elements if the time step becomes too small compared to the original time step (roughly equivalent to a maximum compressive strain criterion). A "crashfront" is then defined from elements sharing nodes with deleted elements. All strength values for elements in the crashfront are reduced by a softening factor, which is empirically determined as the ratio between the crushing stress in a tube crushing test, and the stress corresponding to first-ply failure under axial compression based on the in-plane failure theory. If effective, this should provide an empirical factor forcing the stress in the crashfront to correspond to the tested value. Considering ply degradation rules, however, it is not clear that softening each of the strength criteria will correspond exactly to limiting the stress in this way. Furthermore, localized buckling of material in the crashfront can derail the effectiveness of this method. Matzenmiller and Schweizerhof [12] show correlations between experimental and finite element results for a 13-ply glass/vinylester tube using LS-DYNA. A remarkable agreement is shown. The authors note, however, that agreement was due to the ability of the model to capture the "local folding" failure mechanism seen in the experiment. It is not clear how effective the approach would be for splaying type failure mechanisms, in which delamination plays a larger role in the response and the deformed shape may play a role in stabilizing the material in the crashfront. Results of a similar model, this time of a tube triggered by an internal plug triggering mechanism, are presented by Kerth and Maier in Reference 14. While the agreement with experimental results is shown to be good, the authors note that a reason for the discrepancies that exist is that, "the material model implemented ...cannot explicitly take into account delamination." An apparently similar model is shown by Castejón et al [15]. However, almost no details about the modeling techniques are given.

Some recent efforts have attempted to introduce strain rate effects into the modeling of composite structures. Feillard [16] modeled foam-filled e-glass/vinylester composites using a modified Johnson-Cook mechanical law, with properties based on high rate tensile tests of the glass mat material. Good correlations between experimental and finite element results are shown for tubes specimens. However, the author notes that modeling problems remain relative to accurate modeling of the bonding between the composite and the foam. Furthermore, it is not clear how applicable this approach would be to composite systems other than the glass mat used in the study. Philipps et al [17] present work on characterizing the response of composites to high strain rates for application to crash models.

As noted above, there has been some success in modeling crushing of composite using composite damage models based on in-plane characterization of composite laminates. However, considering again the nature of the crushing event typified by the tube specimen shown in Figure 1, it is clear that a coupon tensile test produces a very different response from a crushing specimen. The presence of crushing initiators in crushable structures produces damage at stress levels below that associated with the intrinsic strength of the laminate. Thus, the success of a crush modeling approach based on in-plane failure characterization may be limited to structural concepts in which crushing failure is dominated by a local buckling failure mode. This may be typical for automobile structures. However, higher-performance aircraft structures based on graphite-fiber composites may not be well modeled by this approach.

Phenomenological Modeling of Composite Crushing

The failure and damaging models described above appear to be effective for structures whose failure modes are governed by large-scale laminate failure or local instability. However, these models (or perhaps any modeling approach based on modeling a laminate by a single shell) may be limited in their ability capture the full range of behavior present in the crushing of a composite specimen. Various authors have attempted to produce more detailed models of the crush zone in composite structures. These efforts are reviewed in the following paragraphs.

Perhaps the earliest attempt to model the crushing behavior of composites was reported by Farley and Jones [18]. They used a static finite element model to predict the crushing performance of composite tubes. The laminate was modeled as an assembly of plate elements representing the plies joined by springs representing the ply interfaces. Delamination was predicted using a virtual crack extension technique. Correlation with experimental results was reasonable given the limited phenomenology modeled. Similar models featuring progressive delamination growth were developed by several researchers for more detailed application to crushing analysis. Kindervater [19] describes a quasistatic finite element model used to study the initiation of crushing damage in a composite laminate under quasistatic crushing loads. Initiation and propagation of delamination damage was modeled by predicting failure in resin layers modeled between plies in the finite element mesh. The author, with Vizzini, [20] developed a 2-D, quasistatic finite element model applicable to the crushing of composite plates. Delamination between plies was modeled based on strain energy release rates computed using the virtual crack closure technique. The model qualitatively captured some of the physical behavior of plate crushing, but due to the limited failure phenomenology included in the model did not yield accurate predictions of crushing stress. Hamada and Ramakrishna [21] developed a finite element model for the crushing of composite tubes that exhibit a splaying failure mode, in which a single primary delamination divides the laminate into two fronds that are forced away from each other by a wedge of compacted debris. The initial finite element mesh included a representation of a pre-existing debris wedge and delamination crack. Extension of the central crack separating the fronds was predicted by calculating a stress intensity factor, K, at the crack tip. This approach is limited by its reliance on a predefined crush zone morphology and linear computation as well as by limitations in the fracture mechanics used in the model.

More recently, finite element crash codes have been used to make detailed models of laminate crushing. Bolukbasi and Laananen [22] modeled the crushing of a graphite/epoxy plate using an enhanced version of the implicit code NIKE3D. Their model was essentially a rectangular mesh of solid elements. An initial crack was assumed at the midplane of the laminate, and due to the assumption that the resulting deformation would occur in a splaying mode only one half of the laminate thickness was modeled. Strain energy release rates were calculated and used to predict delamination at various ply interfaces. Boundary conditions near the outer supports were released following failure of the material near the sides of the elements to mimic the physical supports in the plate crushing test that was being modeled. The authors show a good correlation between the computed and experimental crushing stresses, while noting that their results were sensitive to the friction coefficient used for contact between the composite plies and the steel crushing surface. Kohlgrüber and Kamoulakos [6] modeled the crushing of a composite semi-circular laminate using the finite element crash code PAM-CRASH. The laminate was modeled by discretizing each ply separately. Plies were held together by multipoint constraints.

Delamination growth was predicted based on the forces resulting from the constraints. The model showed qualitative agreement with experiments in terms of the deformation shape, though the crushing force was underpredicted. Boonsuan [23] made some preliminary attempts to model the initiation behavior of graphite/epoxy composite plates under crushing loads using MSC.Dytran. The results showed a strong relationship between assumed initial delamination geometries and subsequent deformation shapes in the crush zone. Tay et al [24] present some of the most detailed models of the crush phenomenology of composite laminates to date. They modeled a detail of the crushing zone for a carbon/PEEK composite. The models are phenomenologically based, and use an initial mesh that is designed to trigger a splaying type deformation mode. Because solid elements are used, there is a practical limitation to the number of ply delaminations that can be modeled. The authors permitted delaminations at a smaller number of interfaces than existed in the physical structure (20 plies). Axisymmetric and 3-D models of a portion of the ring of a tube structure were made using ABAQUS. Delamination growth was predicted based on the tensile and shear forces generated by tied connections connecting nodes on opposite sides of a laminate interface. Reasonable agreement with experiments is achieved. However, the authors note that the goal of accurately modeling the crushing behavior of a composite "does not yet appear to have been achieved."

The models described above demonstrate the potential as well as the limitations for modeling composite crushing behavior by using finite element models based on simplified crushing phenomenology. Good correlations are obtained in many cases using models that do not fully capture all aspects of crushing damage observed experimentally, provided sufficient attention is given to the aspects of crushing that most directly control the response. However, even if highly detailed models of laminate crushing were practical for modeling a composite laminate or tube test, such an approach would still be unlikely to be effective for crash analysis. The relevant length scales of a detailed crushing model would need to be on the order of the ply thickness (to account for delamination or the formation of ply bundles, for example). Therefore, the computational burden imposed on a large structural model by the inclusion of detailed modeling of crushable elements would be tremendous.

Hybrid Analyses

Hybrid modeling techniques have been used to incorporate experimental crush modeling data into crash analyses. By this method energy-absorbing components are modeled by way of one-dimensional spring elements whose properties are derived from tube crush test data, for example, rather than attempting to model complex crushing behavior directly. Such an approach is employed in crash codes such as KRASH or DYCAST [7]. In principle, it is possible to implement this modeling strategy into a detailed finite element crash model. However, success of this method depends on the ability to treat the energy absorbing elements as discrete members that do not otherwise effect the response of the structure. If an energy-absorber has a dual role, such as serving as a floor beam that transmits bending moments across the structure in addition to absorbing energy, there is difficulty in applying this method. Also, this method may not properly identify failure modes such as global buckling of an energy absorbing element, or other global failures, and it may be difficult to properly account for the effects of differing loading conditions on the response of the energy absorbing members.

PRESENT RESEARCH

Based on a review of previous laminate crushing modeling efforts, it is clear that an alternate approach is needed for practical modeling of composite crushing as part of a crash analysis of a vehicle structure. The present research studies an approach to modeling laminate crushing through a variation on the hybrid modeling approach described above. Here, hybridization based on experimental crush test data will occur on an element level rather than on the level of an entire structural subcomponent as with earlier hybrid models. The method is similar to models based on in-plane fracture laws and the Composite Damaging model described in References 12 and 13. However, in the current approach, when crushing is predicted in an element the response of the complete laminate will be governed entirely by test data from laminate crushing tests rather than continuing to use conventional ply or laminate failure data. Ply-by-ply analysis and failure criteria are then no longer considered. Both laminate crushing response (obtained using tube or plate crush test specimens) and conventional ply failure properties will be used to define the response of an element. Typically, the hybrid elements behave as conventional composite shell elements. The stress state is monitored, however, and if threshold values are exceeded, the element properties are altered to behave in a fashion consistent with the crushing properties of the composite laminate. To mimic the behavior of crushing initiators in composite specimens or composite structural configurations, a switch is assigned to each element. This switch is initially active for elements located in proximity to crushing initiators, and is activated in adjacent elements when crushing conditions are predicted in an element. In this way, simulated crushing damage can able to progress through a laminate, but crushing will not be self-initiating in all elements. Thus, large stresses occurring away from sites of existing crushing damage will lead to conventional ply failures, rather than simulated crushing damage in that region.

The use of this hybrid element technique necessitates conducting laminate crushing tests as part of a composite structural modeling technique. Laminate crushing tests are relatively easy to conduct, and therefore may not present a substantial additional testing burden, though the possible need for dynamic crush testing will increase the expense. However, because physical models of crushing damage are not foreseeable for general crashworthy composite structures, this burden may be unavoidable if the benefits of crash modeling are to be enjoyed.

The present research is comprised of experimental and computational aspects. The experimental portion of the program is directed toward obtaining the necessary crush test data for use in the computational studies and to generate test data for validation purposes. Quasistatic plate crush testing using a test fixture as described in NASA CR-4526 [25] is used for basic input data. Test articles based on a different test geometry are developed to provide data useful for validation of computer models. The test article is intended to be simple in geometry, yet offer sufficient modeling complexity to thoroughly test the capabilities of the modeling procedure. Interaction between conventional ply failure, instability effects, and laminate crushing is therefore desirable for these test articles. Column specimens formed by the intersection of flat laminates are used for this purpose. The computational portion of the research involves investigation of the proposed modeling procedure. The procedure is implemented using the Finite Element crash code MSC.Dytran [26]. Models of simple structural geometries are made using the procedure. Because of difficulty in implementing the procedure, only simple configurations are studied. In addition to studying the proposed modeling procedure, the existing LS-DYNA enhanced composite damaging model [12] is studied to evaluate its utility for modeling laminate crushing.

EXPERIMENTAL PROGRAM

The experimental program had two purposes: to provide input data necessary for semi-empirical finite element crash modeling efforts and to provide data for validating computer modeling approaches. The test specimens used include flat plate specimens crushed in a support fixture as described in Reference 25 and X-shaped column ("X-column") specimens representing the intersection of two flat laminates developed for this effort. The flat plate specimens are primarily needed to generate input data for crush models, though these specimens were also modeled using LS-DYNA, as noted below. The X-shaped column specimens were used to allow crushing of flat laminates without the constraints of the plate fixture and to provide data to facilitate validation of crush modeling procedures. A single material, IM7/8552 unidirectional graphite/epoxy, was used for all specimens. All laminates were based on the $[\pm 45/0]_s$ laminate, which is common among studies of the crushing response of composites. For modeling simplicity, laminates were primarily based on ply-level scaling in which multiple plies at the same angle are grouped together to increase the thickness [27]. As will be noted below, this caused problems with the crushing performance of the specimens due to an increased prevalence of delamination. Some of the X-column specimens were produced using a different lay-up scheme. All specimens were fabricated that the Composites Research Laboratory at the University of Maryland, College Park. The following sections outline the experimental procedures and results from the experimental program.

PLATE CRUSHING

Results from plate specimen testing are summarized in this section. Additional detail may be found in Reference 28, from which much of the discussion in this section is based. Flat plate specimens were crushed using the fixture type described by Lavoie, Morton and Jackson in Reference 27. In this fixture, flat laminates are supported on the sides between knife-edge supports and end loading is introduced through flat loading surface on the top and bottom. For the present research, some modifications were made to the fixture design. The fixture in References 25 and 27 was built to support a scaling study, and could be used with two different plate dimensions. The present fixture was built to accommodate a single specimen width of 89 mm (3.5 inches) between the knife-edge supports. To reduce machining costs, and to avoid expensive refurbishment costs if the crushing surfaces of the loading fixture are degraded due to use, removable inserts of hardened steel were used for the crushing and loading surfaces while easier-to-machine medium low-carbon steel was used for the other flat surfaces of the fixture. Rather than using shims to adjust the thickness between the knife edge supports, set-screw were manufactured into the fixture to allow continuous adjustment of the knife-edge supports up to a maximum specimen thickness of about 5 mm. A photograph of the modified fixture is shown in Figure 2. The removable hardened steel surfaces are visible above and below the specimen. Set screws for adjusting the knife edge supports are visible on the central vertical rods.

Specimens were crushed under quasistatic loading conditions using a 267kN (60 kip) capacity hydraulic testing machine. The testing machine is manually controlled. Average loading rates are displayed on a computer monitor during the test, and the controls are adjusted to achieve the desired quasistatic displacement rate. In practice, the desired loading rate could be achieved within a few minutes. Because of the slow loading rate and the duration of the tests, most of the measured crushing response is therefore at the desired loading rate. Load was measured using a

133 kN (30 kip) capacity load cell ported through a digital indicator to provide an analog voltage output. A LVDT with a total stroke of 6 inches was used to measure the overall stroke of the testing machine. Data were collected and recorded using LabVIEW data acquisition software. A schematic of the testing set-up is given by Figure 3 [28].

Specimens for flat plate crushing were fabricated from IM7/8552 graphite epoxy. Specimens were initially manufactured to dimensions of 102×140 mm (4×5½) inches, with a machined in steeple chamfer along one edge. A schematic of a typical specimen as manufactured is given in Figure 4(a) [28]. Specimens were manufactured in the following lay-ups: $[(\pm 45)_2/0_2]_s$, $[(\pm 45)_3/0_3]_s$, $[(\pm 45)_3/0_6]_s$, and $[(\pm 45)_2/0_5]_s$.

Plate Crushing Results

Initial crush testing using the simple steeple chamfer (Figure 4(a)) showed poor performance. During initial loading, large delaminations popped in between the ±45° and 0° ply groups. Subsequent response was dominated by large-scale instability rather than a desirable progressive crushing failure mode. Trigger modifications were pursued to improve the initiation. Two types of trigger modifications, illustrated in Figure 4(b) and 4(c), were used: notches and slits, both used in conjunction with the existing steeple chamfer. The crushing response was considerably improved by the trigger modifications, as illustrated by representative load-displacement curves for the $[(\pm 45)_2/0_5]_s$ laminate with each of the trigger types shown in Figure 5 [28].

For either the slit- or notch-modified triggers, the resulting failure mode was essentially a splaying mode, in which the ±45° ply groups moved away from the centerline essentially intact while the 0° plies, contained by the fronds formed by the angle ply groups, were more heavily damaged. Relatively little damage other than tearing at the location of the knife edge supports is evident in these sublaminates. This behavior is different than is observed in other similar crushing specimens using different graphite/epoxy systems. For other graphite/epoxy specimens, substantial splitting between fibers is observed in angle plies [2,29]. The present behavior may be due to the matrix material used (Hexcel 8552 epoxy), which is categorized as a "Mid-Toughened" epoxy resin system. It is not clear that this was ultimately beneficial for the crushing response. Indeed, the energy absorption performance of the present specimens is relatively low as compared with other graphite/epoxy systems, as will be shown below.

The specific sustained crushing stress (SSCS) is defined according to standard practice [1,2] as:

$$SSCS = \frac{P_{ave}}{\rho A},$$

where P_{ave} is the average crushing load during sustained crushing, ρ is the density of the material, and A is the cross-sectional area. The SSCS may be considered to be the energy absorbed per unit mass of material available during sustained crushing. The trigger ratio is defined as the ratio between the maximum load during triggering and the average crushing load. In one case, no clear peak initiation load could be identified, and hence no peak load or trigger ratio is reported in Table 1. No results are presented in Table 1 for the $[(\pm 45)_3/0_6]_s$ laminate, for which no successful crush tests were completed. Table 1 compares SSCS for all specimens

tested based on the trigger used[2]. For the $[(\pm 45)_3/0_3]_s$, the results are insensitive to the trigger used. For the $[(\pm 45)_2/0_5]_s$ laminate, the results are fairly consistent for the modified triggers (notch, slits), but poor for the simple steeple chamfer. The values of SSCS determined for these laminates are consistent with values of SSCS for graphite/epoxy systems reported by other researchers, which vary between about 40 and 100 kJ/kg [29-31]. Thus, although the failure mode is somewhat unusual, the overall response is consistent with other researchers, suggesting that the triggers used in this study produced adequate crushing response.

X-COLUMN SPECIMENS

Column specimens with an "X-shaped" cross-section were produced to explore the crushing behavior of flat laminates without the restrictions of the crushing fixture used for plate specimens, and to collect data that can be used to validate modeling efforts. A photograph of a typical specimen of this type is shown in Figure 6. The testing procedure for this type of specimen is essentially similar to that used for tube crushing. The test specimen is similar in some respects to the "cruciform" specimens described in Reference 6 and is similar to specimens used to study "subfloor intersections" in Reference 32. However, the cruciform elements in References 6 and 32 contain special intersections for attaching intersecting beam-like segments. In Reference 6, the intersection produces a tube-like geometry. In Reference 32, various attachment types are considered, essentially acting as splice plates between intersecting beams with "C-channel" shapes. The studies in References 6 and 32, and similar studies using sandwich beams [33], were directed toward structural applications. The present specimen is intended to explore the crushing of flat laminates, and contains no additional structural material at the intersection. Rather, a planar junction at the intersection is achieved through the manufacturing process. Notice in Figure 6 that no mechanical or adhesive fastening is used to join the intersecting laminates in the specimen.

Specimen Manufacturing

A manufacturing procedure was developed using wet lay-up composites to produce initial prototype specimens then modified for graphite/epoxy preimpregnated tape. Specimens are laid up on a four-piece aluminum mold shown in Figure 7. The lay-up procedure is illustrated in Figure 8 for the wet lay-up prototype specimens. The lay-up steps are essentially similar when preimpregnated tape is used. Angle plies are continuous along adjoining angles of each segment of the mold as shown in the first picture in Figure 8. Axial plies are then added before adjoining segments of the mold are joined. Pins are used to assist the alignment of the mold segments. The completed mold is then placed in an envelope vacuum bag and cured. Specimen curing for the prepreg specimens is conducted in an autoclave whereas the wet lay-up prototypes were allowed to cure under ambient conditions. Specimens were trimmed using diamond grit tooling to the nominal specimen dimensions shown in Figure 9 (note that various lengths were used for the specimens tested here). Triggers were added at Florida Tech.

[2] This table is derived from Reference 28. Data for the $[(\pm 45)_3/0_3]_s$ lay-up have been corrected from data in Reference 28 by fixing a calculation error from the data contained therein.

Two sets of graphite/epoxy prepreg x-column specimens were manufactured from IM7/8552 graphite/epoxy at the Composites Research Laboratory at the University of Maryland, College Park. One set of specimens with a lay-up of $[\pm 45_3/0_3]_S$ was produced in specimen lengths of 102 mm (4 inch) (2 specimens) and 76 mm (3 inch) (1 specimen). These specimens are designated X1-1, X1-2 and X1-3. A second set of specimens with a lay-up of $[(\pm 45/0)_3]_s$ was also produced with 3 specimens with a 76 mm (3 inch) length, and one with a 51 mm (2 inch) specimen length. These specimens are designated X2-*n*, where *n* is the specimen number.

The intent for the X-column specimens was to use the same material and lay-ups as tested in the plate crushing fixture. As noted above, effective triggering was difficult with these specimens, and it is expected that triggering would be even more difficult with the X-column specimen arrangement. Preliminary testing of X-column specimens using a steeple chamfer showed very poor results. Crushing was not initiated, and global instability of the test part occurred. In addition, the steeple chamfer was difficult to install on the X-column specimens. The nominal trigger configuration selected for the remaining X-column specimens was therefore a plain chamfer configuration as shown in Figure 10. This type of chamfer is easy to machine, and it was hoped that this configuration would initiate greater crushing damage in the angle plies and reduce the tendency toward large-scale delamination response. This is verified, to an extent, by testing one of the $[(\pm 45)_3/0_3]_S$ plate specimens with the plain chamfer and comparing results from other trigger types. Figure 11 compares load displacement results for this lay-up using plain chamfer and steeple chamfer. The peak load is greatly reduced for the plain chamfer while the subsequent response is largely similar. Chamfer was introduced in the specimens using a hand-held rotary tool, and thus there was noticeable variability in the results, and it was not possible to achieve the desired "sharpness" in the trigger region. The "point" of the trigger was typically somewhat blunt compared to the desired angle. Because chamfer cannot be introduced at the intersection, all material was removed from the center of the specimen to the nominal depth of the chamfer. For symmetry, the chamfer was applied to a consistent edge moving clockwise around the specimen. The nominal chamfer configuration can be seen in the photograph of a typical specimen shown previously in Figure 6. Because of the propensity toward global instability in the plate column specimens, it was essential that effective triggering be achieved. Indeed, this was not always the case, and specimens were modified to promote more effective crushing. This included altering the trigger, reducing the width of the long legs of the cross-section on some specimens, and altering the specimen length.

To evaluate the test specimen, samples were prepared from unidirectional IM7/8552 graphite/epoxy with two lay-ups, $[\pm 45_3/0_3]_S$ and $[(\pm 45/0)_3]_s$. One end of each specimen was chamfered to provide a crushing initiator, and specimens were crushed against a hardened steel surface under quasistatic loading conditions. Variations in the x-column specimen geometry (the length of the specimens and the width of the "legs" of the cross-section) were also made to explore the influence of the specimen geometry on the observed behavior. Due to budgetary limitations, only a small number of test specimens were produced. The number of specimens is sufficient to evaluate the utility of the method, but not necessarily sufficient for thorough statistical representation of the performance of a given material or lay-up.

X-Column Crushing Results

Testing of the X-column specimens with the $[\pm 45_3/0_3]_S$ lay-up was disappointing. Triggering produced large-scale delaminations, perhaps greater than were observed in the plate specimens, and instability dominated the response. For the specimen with normal cross-section dimensions, a steeple chamfer, and a four-inch length (X1-1), the response is illustrated in Figure 12. The peak load for this case was below 5kN, and the test was halted. Because triggering was poor in this first test, trigger modifications were pursued as with the plate specimens. The chamfer in specimen X1-2 was modified by the addition of slits, spaced similarly to those used previously in the plate specimens. This was not effective, particularly due to instability effects at the free edges of the specimen, as illustrated in Figure 13. Specimen dimensions were studied by modifying the damaged specimen X1-1. Damaged material was removed from one end, and the width of the longer arms was reduced to discourage buckling. The resulting specimen, designated X1-1b, had nominal dimensions as shown in Figure 14. A plain chamfer trigger (Figure 10) was used for this case. Crushing performance was improved compared with the X1-1 test, but large delaminations and local instability still dominated the response. Specimen X1-3 with plain chamfer likewise initiated in a mode dominated by local instability near the crushing surface, and large delaminations between the ply groups. Crushing was allowed to proceed in this specimen to determine whether progressive crushing damage would develop. The sequence of damage in this specimen is illustrated in Figure 15, which shows the predominance of instability in the response, and the presence of delaminations growing the entire length of the specimen. Following crushing, the angle plies sublaminates were largely intact. Load-displacement curves for the three specimens of this type are shown in Figure 16. The high initial peaks in each of the cases illustrate the ineffectiveness of the triggering for these cases. Although it was expected that instability would be a significant issue with these specimens, based on the results of the plate crushing tests effective triggering should have permitted more favorable response. For purposes of comparison, specific sustained crushing stress values were computed based on the load-displacement curves in Figure 16. These results, as well as those for other X-column specimens, are summarized in Table 2. It should be noted that the failure modes observed are not true progressive crushing modes, and the extension of delaminations along the entire length of the specimen renders these values of SSCS specific to the specimen length tested only, and they are not reliably representative of the material and lay-up. The results are low as compared with the plate crushing results for the same material using a similar lay-up. Values of SSCS for the $[(\pm 45)_3/0_3]_S$ lay-up tested in the plate crushing fixture ranged from 45-61 kJ/kg for the various triggers used, as described above. Note that for specimen X1-1b, two values of SSCS are reported, the first based on the portion of the curve from 10-22mm crushing displacement, before the substantial load drop due to an instability that occurred at about 22mm of crushing displacement, and the second including all post-initiation data.

Although the initial intent was to use laminates for which plate crushing data were available for the X-column specimens, the poor performance of the X1 specimen type demonstrated that a different lay-up was necessary for the remaining tests. Although instability could be managed by altering the specimen dimensions, the prevalence of delamination and its detrimental effects on the response could only be controlled by altering the lay-up. A distributed lay-up with smaller thickness of ply groups would reduce the tendency toward delamination. Thus, the second set of specimens was fabricated with a $[(\pm 45/0)_3]_s$ lay-up.

The performance of the $[(\pm 45/0)_3]_s$ specimens was markedly improved over the previous specimen type. Triggering was much more effective, although delamination and ply separation remain key features of the crushing response, as in the plate specimens. The scale of the delaminations was greatly reduced for the $[(\pm 45/0)_3]_s$ lay-up as compared with the X1 specimens, and the overall level of damage in the specimens was considerably greater. This is reflected by the significantly higher SSCS values reported in Table 2. No value of SSCS is reported for specimen X2-1 because due to the short specimen length, splitting between plies reached the full length of the specimen before sustained crushing was observed. The substantially increased SSCS for specimen X2-3 which has reduced cross-section dimension compared to the other X2 specimens, is due to the increased stability of the specimen, indicating that the specimen fulfills the purpose of presenting behavior that contains both crushing and instability response within a single specimen. Load-displacement curves for all X2 specimens are given in Figure 17.

Discussion

For the material tested, in both the column specimens and using the flat plate crushing fixture, crushing (when it occurred in the absence of global buckling) was predominately in a splaying mode. Delamination at the interfaces between the angle plies and the axial plies allowed the formation of fronds of material that stayed largely intact during testing. The IM7/8552 material proved to be very resistant to damage. Even when a frond of material was bent to almost a 90° angle with a tight radius of curvature, little cracking or matrix failure was visually evident. This is illustrated in Figure 18, which shows a detail of the crushing response from specimen X2-3. Axial fibers near the center of the laminate, particularly near the intersection in the column specimens were more highly constrained and experience substantially more fracture with a smaller characteristic debris size (see Figure 19). The overall crushing behavior of the X-column specimens was relatively complex, with variations of failure behavior from specimen to specimen or even between different arms of the same specimen. Figure 20 shows a detail of crushing damage at approximately the same displacement level on each of the four arms of specimen X2-2. Note that pairs of "legs" have different widths on this specimen. In these pictures, it is seen that the while the behavior is similar for each of the two narrow sides of the specimen, and for each of the two wider sides, that the response of the narrow and wide sides of the specimen is different. In particular, the length of the delaminations is longer on the wider sides, and damage is greater near the central part of the laminate on the narrow sides. As is expected from plate buckling theory, instability is a greater factor when the arm width is larger. On several occasions, the failure mode observed in a single arm of wider dimensions would involving local buckling or failure of the complete laminate thickness, such as is shown in Figure 21.

The ability to alter the crushing mode and to promote interaction between crushing and instability was a goal of the specimen design. This is intended to present a challenge for crush modeling efforts and to allow data to be collected to validate crushing models and to determine their ability to distinguish between laminate crushing and instability-dominated failure modes. One of the most interesting aspects of the X-column crushing specimen from the standpoint of providing data for the validation of finite element crushing models is the ability to observe the evolution of crushing damage in real time as the test progresses, rather than only through postmortem sectioning and inspection. Because of the nature of the free edge in the specimen,

the progression of damage through the laminate thickness that would be hidden in a tube specimen is visible, at least in part. Figures 18–21 graphically illustrate the level of detail of observation of crushing damage that can be made. A more complete picture of the crushing of an X-column specimen is given in Figure 22, which illustrates the crushing of specimen X2-2 over a total crushing displacement of over 40mm. This sequence of photographs illustrates damage in different portions of the specimen at different points in the loading sequence from damage initiation to post-mortem study. A variety of failure processes are evident in the photograph, allowing quantitative analysis of these mechanisms.

FINITE ELEMENT MODELING

ENHANCED COMPOSITE DAMAGING MODEL

Because the Enhanced Composites Damaging (ECD) model contains features similar to the proposed modeling technique and to get a better understanding of current composite crush modeling capabilities, study of LS-DYNA's Enhanced Composites Damaging Model [12] was made.

For initial study of the method, models of laminated plates crushed in the plate crush test fixture described above were made. Details of the modeling procedures may be found in Reference 28, from which much of the present section is derived. Because the experimental plate crush data are directly used in the ECD model via the "SOFT" parameter that reduces ply strengths in the crashfront, it should be expected that there would be a strong correlation between the experimental and finite element results for the simple laminated plates. This is indeed the case, as can be seen in Figure 23 from Reference 28, which compares load-displacement results between the experiment and the LS-DYNA model for one lay-up, and Table 3 [28], which compares finite element and experimental results for all lay-ups for which experimental results are available. Examination of the finite element displacement shapes, however, suggests caution in evaluating the success of the model. Typical deformed shapes are shown in Figure 24. Note that the response is largely driven by local instability of the laminate near the crushing surface. Little action of the crashfront procedure is evident, and only a small number of elements are deleted following initiation. The primary action of the crashfront procedure appears to be in limiting the load level prior to the onset of instability. Thus it is clear that although the quantitative values produced by the model are reasonably accurate, the model does not accurately predict the crushing behavior.

A more difficult test of the ECD material model is made by modeling the crushing of graphite/epoxy truncated cones [34,35]. In these previously published tests, truncated cone specimens of various taper angles were loaded in an off-axis fashion by cutting the ends at an angle to the cone axis. The cone specimens were then loaded between their ends under quasistatic crushing loads. Figure 25 (from Reference 35) contains a schematic drawing of the cone geometry. A photograph illustrating the experimental test is given in Figure 26. Note the appearance of splaying behavior wherein the laminate separates into two major portions, one of which is forced into the interior of the specimen, and the other which moves away from the specimen. Because of the off-axis loading condition, damage is not uniform around the perimeter of the specimen [35]. A typical deformed shape for the same case modeled using LS-DYNA's ECD model is shown in Figure 27. The model fails to accurately capture the response of the experimental cone. The model exhibits instability of elements in the trigger region followed by folding behavior, as shown in Figure 27. In the LS-DYNA model, the crashfront does not progress beyond the first trigger element layers. Maier [36] models the crushing response of a different conical specimen and appears to show a similar disparity between the finite element and experimental deformation shapes. Additional models of these truncated cone specimens were made by Jayachandran and reported in Reference 28. Comparison of load-displacement response between experimental and LS-DYNA models for various cases are given in Figures 28-32 [28]. Comparison of computed SSCS values for the various cases tested are

given in Table 4. Despite poor agreement between the finite element and experimental deformation shapes, the SSCS predicted by the FE models is reasonable. However, as with plate specimens, this favorable comparison appears to be largely due to the "SOFT" factor ensuring that initial folding instability is triggered at approximately the experimentally determined crush stress. Progress of the crashfront is not seen in the LS-DYNA models.

HYBRID CRUSHING ELEMENT

This section describes the development of the proposed hybrid technique to employ conventional laminate crushing data in a finite element crash model. This approach differs from the enhanced composite damaging model in LS-DYNA in that when crushing is detected in an element the behavior of the element changes completely to an empirically derived load-displacement response representing crushing of the complete laminate. No ply-by-ply analysis is conducted following crushing initiation. MSC.Dytran was selected for the present modeling effort. EXCOMP, the user-defined orthotropic failure model for shell composite laminates is used to implement the model. A prototype version of the procedure has been tested for limited cases. An outline of the development steps followed and the current status follows. Although limited success has been achieved with simple models, additional development is needed before the approach can be applied to crash models.

As a first step, models using 1-D spring elements were prepared and implemented through user-defined spring property subroutines to study fundamental aspects of the desired procedure and its implementation within Dytran. In these models, the force displacement characteristic of an element in compression was represented as shown in Figure 33. This is an idealized representation of typical laminate crushing response. The key issue studied by the spring models pertained to the progression of the crashfront. In a process mimicking the triggering and progression of crushing damage in a test, elements adjacent to an element in the crashfront are added to the crashfront when the active crashfront element reached the exhaustion displacement, δ_e. Elements not identified as being part of the crashfront behaved as simple elastic springs. The spring element models were useful for learning how to work with Dytran's user subroutine procedures and for identifying modeling issues that would be faced by later models as well. Among the issues identified through the spring element tests are the following: 1) At large crushing displacements the time step becomes small, increasing required computation time. 2) Because of the difference between the element length and the "exhaustion displacement," δ_e, the physical length of the crush zone increases as each element is fully crushed. This causes problems with lateral instability of the stack of crushed elements. 3) Numerical instabilities are possible as a result of the knee in the load-displacement curve around δ_e. Following the initial work with the spring elements, attempts were made to use these spring elements directly in conjunction with composite shell elements to produce the desired crush modeling procedure. However, this method failed to produce a useful model primarily because of problems in implementation through the user subroutines. It was not possible to effectively pass data between shell and spring elements. Therefore, the next step was to model the crushing response entirely using shell elements.

The primary difficulty with this approach relates to the need to switch between conventional laminate behavior and averaged crushing behavior within an element. Whereas conventional composite shell elements use properties defined on a ply-by-ply basis, the crushing element

should have a bulk property defined only for the entire laminate thickness. To overcome this problem, a modeling approach is used whereby parallel meshes of elements sharing common nodes are used. One mesh contains conventional composite shell elements. The other mesh uses specialized shell crushing elements with a stress-strain response similar to the idealized crushing curve in Figure 33 for loading in a preferred crushing direction only. Initially, all elements in the conventional composite mesh are active, and obey their standard stress-strain response; and only a single layer of crushing elements is active. Inactive crushing elements possess only a marginal stiffness. When a trigger element is fully crushed, a signal is sent to the adjacent composite element to kill it, and simultaneously a signal is sent to the adjacent crush element to activate it and have it take over the stress carried by the depleted trigger element. In this way, crushing may be triggered throughout the mesh in a progressive fashion. A schematic drawing of the meshing concept is shown in Figure 34(a). Dashed lines indicate nodes that are shared by elements in the two meshes. Considering only the numbered column of elements in Figure 34(a), initially all normal shell elements (N1-N5) are active, but only crushing element C0 is active. If the maximum crushing strain in element C0 is reached, elements N1 and C0 are deleted and element C1 is activated. Some difficulties were found using this method in the form of Figure 34(a). Because the maximum crushing strains are desired to be extremely large, the time step of the solution will become very small as a C*n* element reaches its maximum strain. Also, if a crushing element is deleted at a relatively small strain (such as 50%) spurious dynamic effects will be introduced as the mesh above the deleted element relaxes and is then reloaded upon the initiation of contact with the following elements. To overcome these difficulties, two offset meshes of crushing elements are used, as illustrated in Figure 34(b). By this approach, the initially active trigger element $C1_1$ will be exhausted when it reaches 50% crushing. Then, element N1 and $C1_1$ are deleted and $C2_1$ is activated. Element C21 will immediately pick up the crushing stress carried by element $C1_1$ prior to hand-off. If $C2_1$ subsequently reaches 50% crush, it will deactivate itself and element N2 and will activate crushing element $C1_2$.

Development and evaluation of a procedure to implement this modeling scheme was implemented using the EXCOMP procedure in MSC.Dytran. Results were first generated using a simple coarse mesh of a flat pate using material property data typical of graphite/epoxy. Due to difficulty with transferring information between elements, the normal crushing elements were programmed into the same EXCOMP subroutine defining the crushing elements. Because of difficulties in programming failure criteria into the user subroutine, the "normal" composite elements used in this models contain linear elastic plies (no failure).

Results are shown in Figures 35 through 39. Figure 35 shows displacement shapes for the simple coarse plate model illustrating the potential for modeling large crushing displacements. A rigid wall, not visible in the figure, is included at the bottom of the model and load is introduced through a constant velocity constraint at the top of the model. No other boundary conditions are applied. Force versus displacement is shown in Figure 36 for this model. This force is obtained from Dytran as the rigid wall contact force. Viscous damping (VDAMP) was used in the model to reduce the fluctuations in the load response and produce a result more representative of a quasistatic crush test. A number of load spikes are evident in the complete load-displacement curve shown in Figure 36(a). These result from two events: 1) the element in the crush front in the lagging crush mesh retains some nominal stiffness while it is not being crushed. Initial contact between this element and the rigid wall produces a load spike, and 2) handoff between

crashfront elements in the C1 and C2 crushing meshes correlates with load spikes. This noise was initially very troubling, and was studied in greater detail. Figure 36(b) shows a portion of the wall force versus displacement curve highlighting a single handoff event, with data collected more frequently than in Figure 36(a) to better illustrate the response. Figure 37(a) shows the stress versus displacement data for the first two crushing elements to impact the wall and Figure 37(b) shows stress versus time for the first plies in the two composite elements nearest the wall. The vertical line around a displacement of 7mm in Figure 37(a) shows the point where element $C1_1$ goes from a crush stress of 100MPa to zero and $C2_1$ simultaneously goes from 0 to 100MPa. From these results, it appears that the load spikes evident in the wall force plot are primarily an artifact of the contact modeling procedure and are not indicative of the magnitude of the response calculated internally to the structure. Problems associated with handoff, however, remain a matter of concern.

To further evaluate the success of the procedure, models of the truncated cone specimens crushed under quasistatic conditions [34,35] are made. (These are the same truncated cone specimens modeled using LS-DYNA and described in the previous section). Because these specimens are relatively simple yet exhibited a range of crushing conditions around their cross-section due to the geometric variation of the loading geometry they make an ideal test case. Only a limited number of truncated cone models were produced. These are 1° taper cones loaded at angles of 5° and 10° relative to their axes (see Figure 25). The loading rate used in these preliminary models is considerably greater than the quasistatic loading rate used in the experimental tests. VDAMP is again used to facilitate correlation between experimental and finite element results.

The displacement history for the 5° cut cone model is shown in Figure 38. This model shows progressive crushing occurring over approximately 50mm of displacement. In the last figure in the sequence, progressive crushing ends and an unrealistic global deformation shape occurs. This results from an artifact of the mesh geometry. Because the test specimens were triggered at both ends, triggers were included on both ends in the finite element model. In the current implementation crush elements must be associated with a single trigger, thus the model is limited to a total crushing depth of 50mm from either end. The awkward deformation shape in the last time step shown results from the lack of a failure model for the composite elements. The finite element load displacement curve shown in Figure 39 is in reasonable agreement with experimental results for small displacements. Note that the experimental specimen suffered a global instability, and toppled over at a displacement of about 20 mm. Prior to this event, the loads are in good agreement. After 50 mm of crushing the finite element load increases unrealistically due to the effect noted above. Results for the 10° cut tube are shown in Figure 40. Progressive crushing is not demonstrated for this case. Failure of the end occurs due to folding of the elements. Better results for this case might be obtained if conventional laminate failure were included in the model. Additional development efforts were pursued, but unexpected difficulties in implementation prevented further progress.

CONCLUSIONS

The problem of laminate crush modeling was addressed through efforts to develop a novel hybrid crush modeling strategy and associated experimental testing.

In the experimental program, IM7/8552 graphite/epoxy specimens were crushed using a plate fixture and through a column specimen with an "X-shaped" cross-section. The x-column test is a useful and simple method for testing flat composite laminates. Stable crushing was achieved using the x-column specimen provided an adequate trigger was present and the overall specimen geometry was such that global buckling was prevented. The X-column specimen provides a relatively simple alternative to plate crushing. Although specimen fabrication is more complex that for plate crushing, no fixture is required and the testing procedures are essentially the same as for simple tube specimens. This specimen is proposed in the present study for purposes of assisting the validation of finite element composite crush models. The benefits of the X-column specimen for this purpose is a greater ability to examine the evolution of damage within the specimen during crushing than is possible with alternate specimen geometries. This is particularly true for materials similar to that examined in this pilot study that crushed in a mode dominated by ply separation and localized instability of sub-ply groups and delaminated elements. In addition, by altering the specimen geometry, the overall stability of the specimen can be altered to make global instability either a crucial part of the response or relatively insignificant. Because of the nature of crush loading in real structures, it is essential for accurate crash modeling that the interaction between global instability and local crushing failure modes be possible to model. This specimen allows such interactions to be studied in a controlled fashion.

Finite element models of laminate crushing were made using the existing Enhanced Composites Damaging model in LS-DYNA and, for limited cases, through a new hybrid crushing element procedure. For simple structural cases, the LS-DYNA models produced good correlation with experimental load-displacement results although the deformation shapes were not accurately modeled. The crashfront procedure contained in the LS-DYNA model did not appear to be effective for the cases modeled beyond initial triggering. Rather, modeled deformation was in a progressive folding mode. Thus, the use of this model as part of a predictive finite element crash model is suspect.

The hybrid crush element shows promise for crush modeling by allowing for direct empirical representation of laminate crushing as part of a finite element model. Substantial issues remain to be resolved before this method becomes a practical alternative for crash modeling. In particular, remaining problems include the following: Off-axis properties of the crush elements must be addressed in a systematic way. In the present models, arbitrary large values of off-axis properties were used. The specific choice of these properties, however, influences the stability of the elements in the crashfront region and can therefore alter the overall crushing behavior modeled. Second, an effective element including conventional ply failure and degradation rules must be developed. This is necessary before complete validation of the modeling approach can be made. Finally, it is observed that the difficulty in implementing the proposed procedures through user subroutines is such that further development would be better implemented with direct access to the source code.

ACKNOWLEDGEMENTS

This research was supported by the NASA Langley Research Center under grant number NAG-1-2260. Lisa Jones was the contract monitor. The author wishes to acknowledge the contributions of Kothandaraman Jayachandran and Frederic Nicot, graduate students in the Florida Institute of Technology Department of Mechanical & Aerospace Engineering.

REFERENCES

1. Hull, D., 1991. "A Unified Approach to Progressive Crushing of Fibre-Reinforced Composite Tubes," *Composites Science and Technology*, 40:377-421.
2. Farley, G. L., and R. M. Jones, 1992. "Crushing Characteristics of Continuous Fiber-Reinforced Composite Tubes," *Journal of Composite Materials*, 26(1):37-50.
3. Fleming, D. C., 2000. "Modeling Delamination Growth in Composites using MSC.Dytran," *Proceedings of the 2nd Worldwide Automotive Conference*, Dearborn, MI, Oct. 9-11, 2000.
4. Haug, E., O. Fort, A. Trameçon, M. Watanabe and I. Nakada, 1991. "Numerical Crashworthiness Simulation of Automotive Structures and Components Made of Continuous Fiber Reinforced Composite and Sandwich Assemblies," SAE Technical Paper Series 910152.
5. Kermanidis, Th., G. Labeas, C. Apostolopoulos, and L. Michielsen, 1998. "Numerical Simulation of Composite Structures under Impact," *Proceedings of the 1998 5th International Conference on Structures under Shock and Impact*, Thessaloniki, Greece, June 1998, pp. 591-600.
6. Kohlgrüber, D., and A. Kamoulakos, 1998. "Validation of Numerical Simulation of Composite Helicopter Sub-floor Structures Under Crash Loading," *Proceedings of the 54th AHS Annual Forum*, Washington, DC, May 20-22, 1998, pp. 340-349.
7. Johnson, A. F., C. M. Kindervater, D. Kohlgrüber and M. Lützenburger, 1996. "Predictive Methodologies for the Crashworthiness of Aircraft Structures, *Proceedings of the 52nd American Helicopter Society Annual Forum*, Washington, DC, June 4-6, 1996, pp. 1340-1352.
8. Johnson, A. F., and D. Kohlgrüber, 1997. "Modelling the Crash Response of Composite Structures," *J. Phys IV France*, Colloque C3, Supplément au Journal de Physique III, (in English) 7:C3-981-C3-986.
9. Faruque, M. and H. C. Wang, 1995. "Crash Analysis of Structures made of Laminated Fibre Reinforced Composites," *Proceedings of the 1995 ASME International Mechanical Engineering Congress and Exposition*, Nov. 12-17, 1995, San Fransisco, CA, AMD-Vol. 210/BED-Vol. 30, pp. 191-201.
10. Lee, H.-K., and S. Simunovic, 1998. "Constitutive Modeling and Impact Simulation of Random Carbon Fiber Polymer Matrix Composites for Automotive Applications," 00FCC-120, SAE, 1998.
11. Tabiei, A., and Q. Chen, 2000. "Micromechanics Based Composite Material Model for Impact and Crashworthiness Explicit Finite Element Simulation," *Proceedings of the 6th International LS-DYNA Users Conference*, Dearborn, MI, April 9-11, 2000, pp. 8-57:8:76.
12. Matzenmiller, A., and K. Schweizerhof, 1991., "Crashworthiness Simulations of Composite Structures –a first Step with Explicit Time Integration," in *Nonlinear Computational Mechanics State of the Art*, P. Wriggers and W. Wagner, eds., Springer-Verlag, Berlin, 1991.
13. Schweizerhof, K., K. Weimar, Th. Münz, and Th. Rottner, 1998. "Crashworthiness Analysis with Enhanced Composite Material Models in LS-DYNA –Merits and Limits," *Proceedings of the 5th International LS-DYNA Users Conference.*
14. Kerth, S., and M. Maier, 1994. "Numerical Simulation of the Crashing of Composite Tubes," *Proceedings of the 4th International Conference on Computer Aided Design in Composite Material Technology*, June 1994, Southampton, UK, pp. 141-148.

15. Castejón, L., J. Cuartero, R. Clemente and E. Larrodé, 1998. "Energy Absorption Capability of Composite Materials Applied to Automotive Crash Absorbers Design," from *Polymer Composites and Polymeric Materials*, proceedings of the 1998 SAE International Congress and Exposition, February 23-26, 1998, Detroit, MI., pp. 37-46.
16. Feillard, P., 1999. "Crash Modelling of Automotive Structural Parts Made of Composite Materials," SAE Technical Paper Series 1999-01-0298, from *Polymer Composites and Polymeric Materials for Energy Management and Occupant Safety*, Proceedings of the 1999 SAE International Congress and Exposition, March 1-4, 1999, Detroit, MI.
17. Philipps, M., L. Patberg, R. Dittmann and H. Adam, 1998. "Structural Analysis and Testing of Composites in Automotive Crashworthiness Application," from *Safety and Material Test Methodologies*, proceedings of the 1998 SAE International Congress and Exposition, February 23-26, 1998, Detroit, MI., pp. 97-101.
18. Farley, G. L., and R. M. Jones, 1992. "Prediction of the Energy-Absorption Capability of Composite Tubes," *Journal of Composite Materials*, 26(3)388-404.
19. Kindervater, C. M., 1995. "Crashresistant Composite Helicopter Structural Concepts - Thermoset and Thermoplastic Corrugated Web Designs," *Proceedings of the AHS National Technical Specialists' Meeting on Advanced Rotorcraft Structures*, Williamsburg, VA, 1995.
20. Fleming, D. C., and A. J. Vizzini, 1996. "Off-Axis Energy Absorption Characteristics of Composites for Crashworthy Rotorcraft Design," *Journal of the American Helicopter Society*, 41(3):239-246.
21. Hamada, H., and S. Ramakrishna, 1997. "A FEM Method for Prediction of Energy Absorption Capability of Crashworthy Polymer Composite Materials," *Journal of Reinforced Plastics and Composites*, 16(3):226-242.
22. Bolukbasi, A. O., and D. H. Laananen, 1995. "Analytical and Experimental Studies of Crushing Behavior in Composite Laminates," *Journal of Composite Materials*, 29(8), pp. 1117-1139.
23. Boonsuan, P., 1996. *Finite Element Modeling of Delamination Growth in Composite Structures*, Master's Thesis, Florida Institute of Technology.
24. Tay, T. E., K. H. Lee, S. Ramakrishna and F. Shen, 1998. "Modelling the Crushing Behaviour of Composite Tubes," *Key Engineering Materials*, Vols. 141-143, pp. 777-790.
25. Lavoie, J. André and J. Morton, 1993. "Design and Application of a Quasistatic Crush Test Fixture for Investigating Scale Effects in Energy Absorbing Composite Plates," NASA CR-4526.
26. Anon., 1999. *MSC.Dytran Version 4.7 Users Manual*, MSC.Software Corporation.
27. Lavoie, J. A., J. Morton, and K. Jackson, 1995. "An Evaluation of the Energy Absorption of Laminated Composite Platesm" *Proceedings of the Institution of Mechanical Engineers Part G, Journal of Aerospace Engineering*, Vol. 209, pp. 185-194.
28. Jayachandran, K., 2001. *Predicting Crush Energy Absorption of Composite Structures using an Explicit Finite Element Code*, M.S. Thesis, Florida Institute of Technology.
29. Fleming, D. C., 1996. "The Energy Absorption of Composite Plates under Off-Axis Loads," *Journal of Composite Materials*, Vol. 30(18), pp. 1977-1995.
30. Carruthers, J. J., A. P. Kettle, and A. M. Robinson, 1998. "Energy Absorption Capability and Crashworthiness of Composite Material Structures: A Review," *Applied Mechanics Reviews*, Vol. 51(10), pp. 635-649.
31. Mamalis, A. G., et al, 1997. "Crashworthy Capability of Composite Material Structures," *Composite Structures*, Vol. 37, pp. 109-134.

32. Jones, L. E., and H. D. Carden, 1989. *Evaluation of Energy Absorption of New Concepts of Aircraft Composite Subfloor Intersections*, NASA TP 2951.
33. Sen, J. K., 1984. "Designing for a Crashworthy All-Composite Helicopter Fuselage," *Proceedings of the American Helicopter Society 40th Annual Forum*, Arlington, VA, May 1984, pp. 56-66.
34. Fleming, D. C., and A. J. Vizzini, 1993. "Tapered Geometries for Improved Crashworthiness under Side Loads" *Journal of the American Helicopter Society*, January 1993, pp. 38-44.
35. Fleming, D. C., 1991. "The Energy Absorption of Graphite/Epoxy Truncated Cones," Master's Thesis, University of Maryland, College Park.
36. M. Maier, 1990. "Experimentelle Untersuchung und numerische Simulation des Crashverhaltens von Faserverbundwerkstoffen," Ph.D. Dissertation, University of Kaiserlautern, 1990, in German.

TABLES

Table 1 Test data from plate crushing specimens, modified from Reference 28

Lay-up	Trigger	Average Crushing Load (kN)	Peak Load (kN)	Trigger Ratio	SSCS (kJ / kg)
$[\pm 45_2/\ 0_2]_S$	Steeple *	-	-	-	-
	Steeple & Notch	20.1	36.8	1.8	57.1
	Steeple & Slits	18.3	32.0	1.7	51.7
	Steeple & Slits	17.1	26.3	1.5	48.5
$[\pm 45_3/\ 0_3]_S$	Steeple	27.6	78.5	2.8	49.9
	Steeple & Notch	34.1	50.7	1.5	61.1
	Steeple & Slits	32.5	63.4	2.0	58.8
	Steeple & Slits	31.4	61.5	2.0	56.0
$[\pm 45_2/\ 0_5]_S$	Steeple	22.3	81.8	3.7	42.2
	Steeple & Notch	52.9	57.3	1.1	99.8
	Steeple & Slits	49.3	-	-	84.0
	Steeple & Slits	53.5	65.3	1.2	99.0

Table 2 Specific Sustained Crushing Stress (SSCS) for X-column specimens

Specimen Designation	Lay-up	Trigger	Height [in]	Nominal C/S Dimensions [in×in]	SSCS [kJ/kg]
X1-1b	$[\pm 45_3/0_3]_S$	Plain Chamfer	2	2×2	37.8, 24.7*
X1-2	$[\pm 45_3/0_3]_S$	Plain + Notch	3	3×2	27.7
X1-3	$[\pm 45_3/0_3]_S$	Plain Chamfer	3	3×2	23.7
X2-1	$[(\pm 45/0)_3]_s$	Plain Chamfer	2	3×2	NA
X2-2	$[(\pm 45/0)_3]_s$	Plain Chamfer	3	3×2	45.7
X2-3	$[(\pm 45/0)_3]_s$	Plain Chamfer	3	2×2	67.4, 62.1*
X2-4	$[(\pm 45/0)_3]_s$	Plain Chamfer	3	3×2	47.6

* Two values given, the first calculated based on performance prior to global failure, the second based on the complete data set, as described in the body of the report.

Table 3 Comparison of experimental and LS-DYNA results for plate crushing [28]

Lay-Up	TEST RESULTS				FE RESULTS			
	Average Crushing Load. kN	Peak Load kN	Trigger Ratio	SSCS kJ/ kg	Average Crushing Load. kN	Peak Load kN	Trigger Ratio	SSCS kJ/ kg
$[\pm 45_2/\ 0_2]_S$	20.1	36.8	1.8	57.1	22.7	50.0	2.2	64.3
$[\pm 45_3/\ 0_3]_S$	34.1	50.7	1.5	61.1	30.0	85.7	2.8	51.2
$[\pm 45_2/\ 0_5]_S$	52.9	57.3	1.1	99.8	35.2	98.5	2.8	66.6

Table 4 Comparison of results for LS-DYNA models and experimental results for truncated cone specimens [28,35]

Lay Up	Taper Angle	Load Angle	TEST RESULTS		FE RESULTS	
			Average Crushing Load. kN	SSCS kJ/kg	Average Crushing Load. kN	SSCS kJ/kg
$[\pm 45/\ 0]_S$	1°	0°	13.1	57.1	11.0	48.1
	1°	5°	14.5	63.0	15.2	66.1
	1°	10°	11.9	51.9	13.7	59.2
	5°	5°	9.4	48.1	8.1	43.8
	10°	5°	7.5	42.1	8.3	46.8

FIGURES

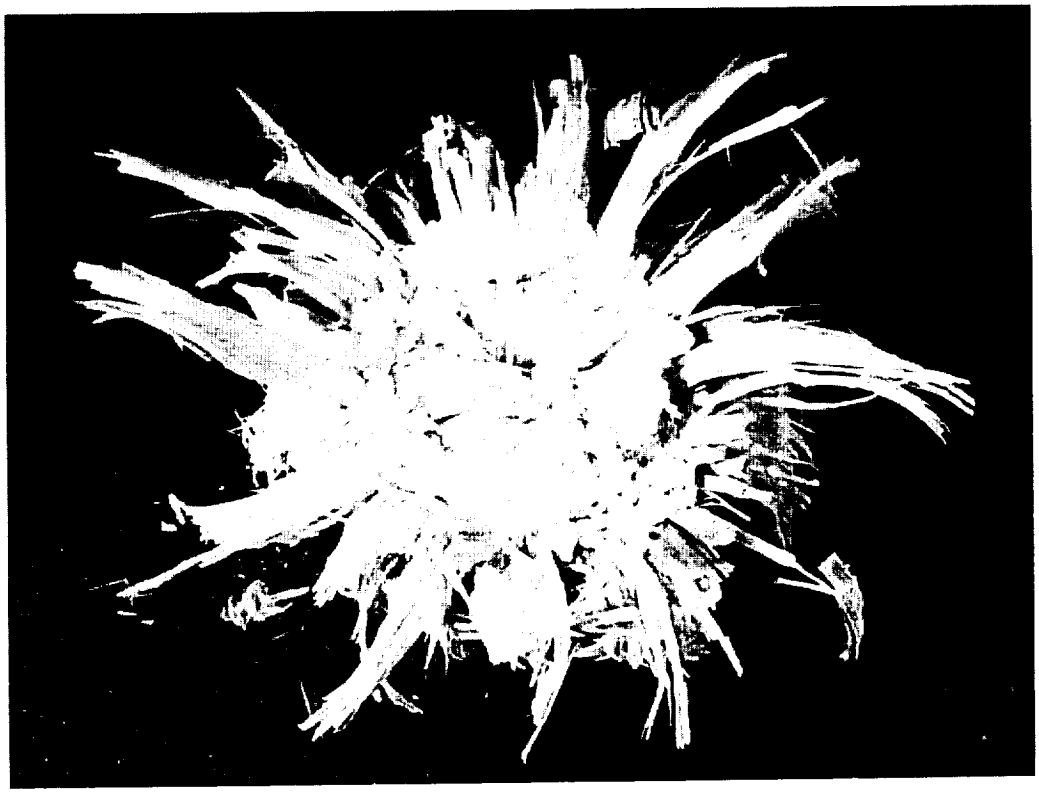

Figure 1 Crushing damage observed in a glass fiber composite tube after load removal

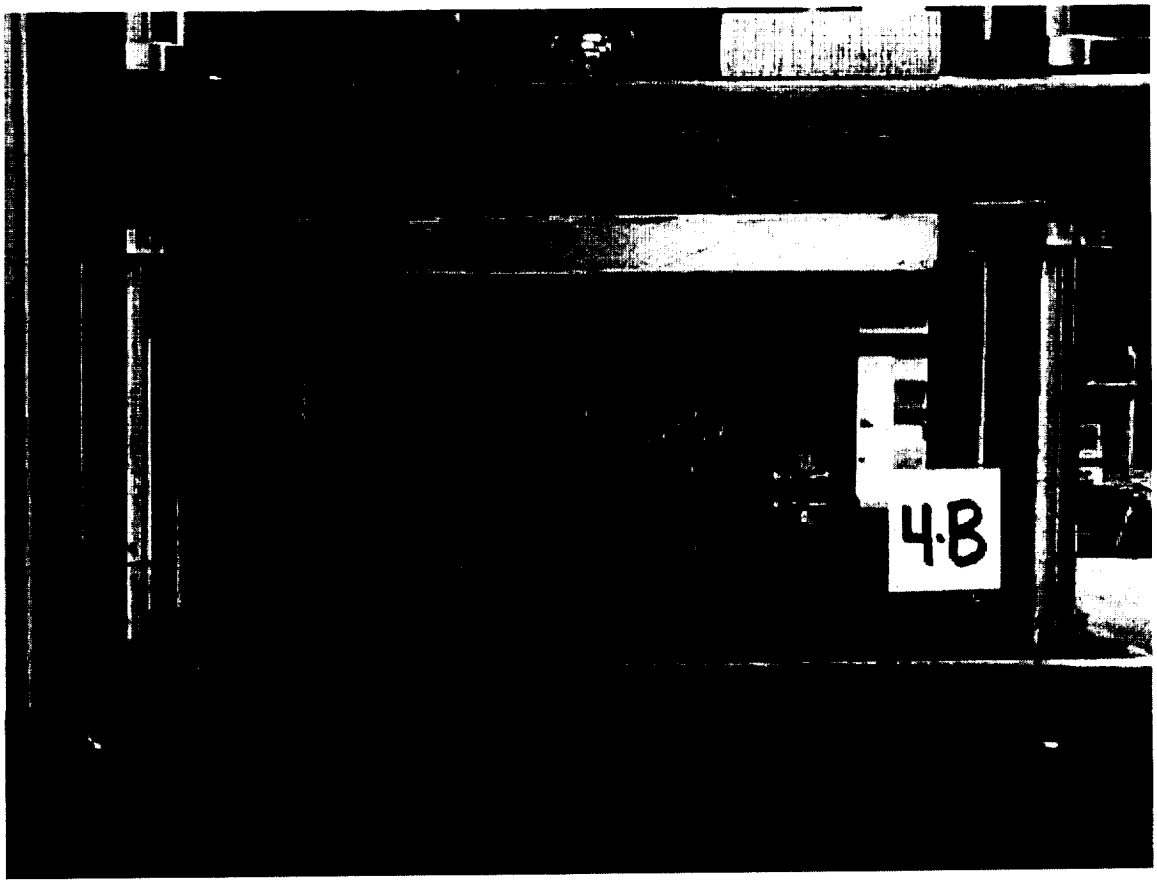

Figure 2 Modified plate crushing fixture based on the design in Reference 25 shown in operation

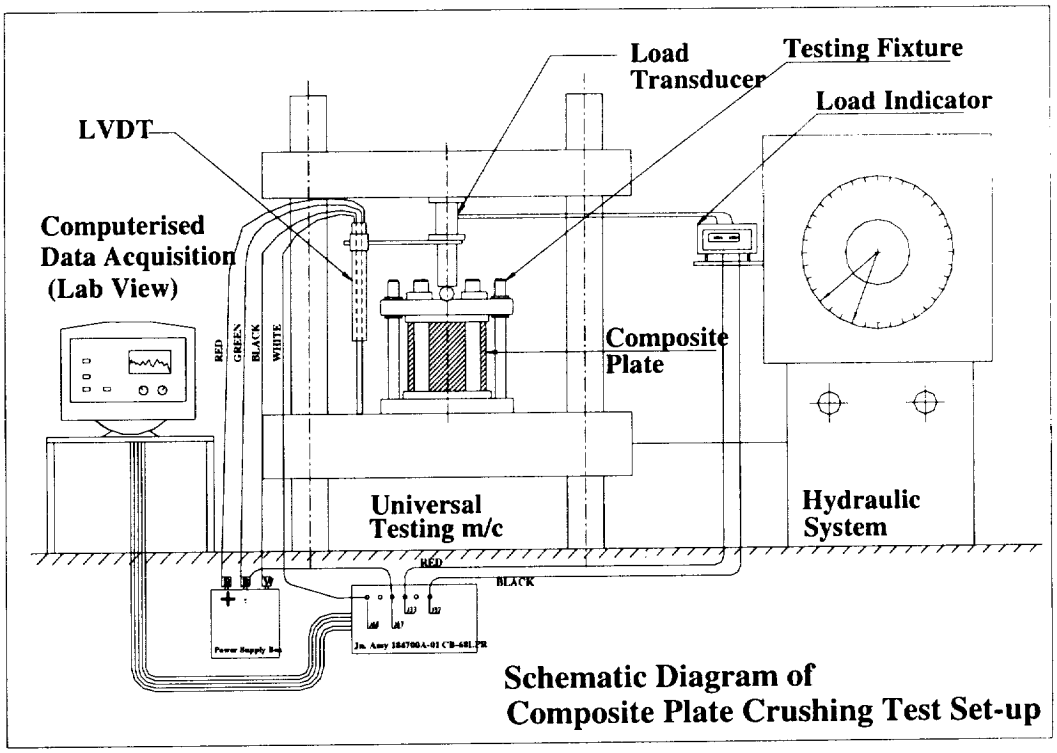

Figure 3 Test set-up for plate crushing (from Reference 28)

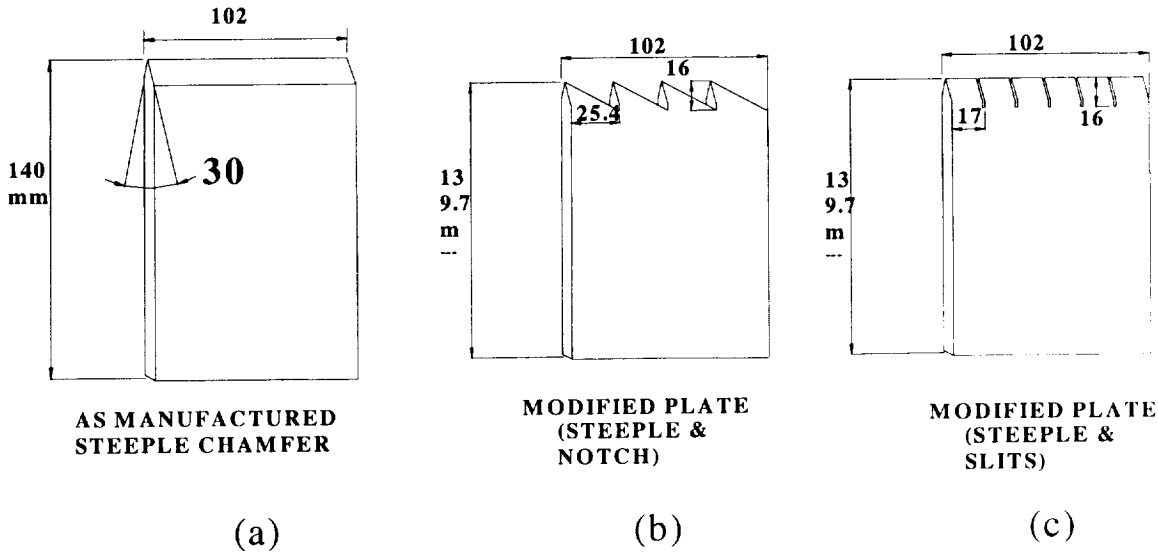

Figure 4 Plate specimen dimensions and triggers [28]

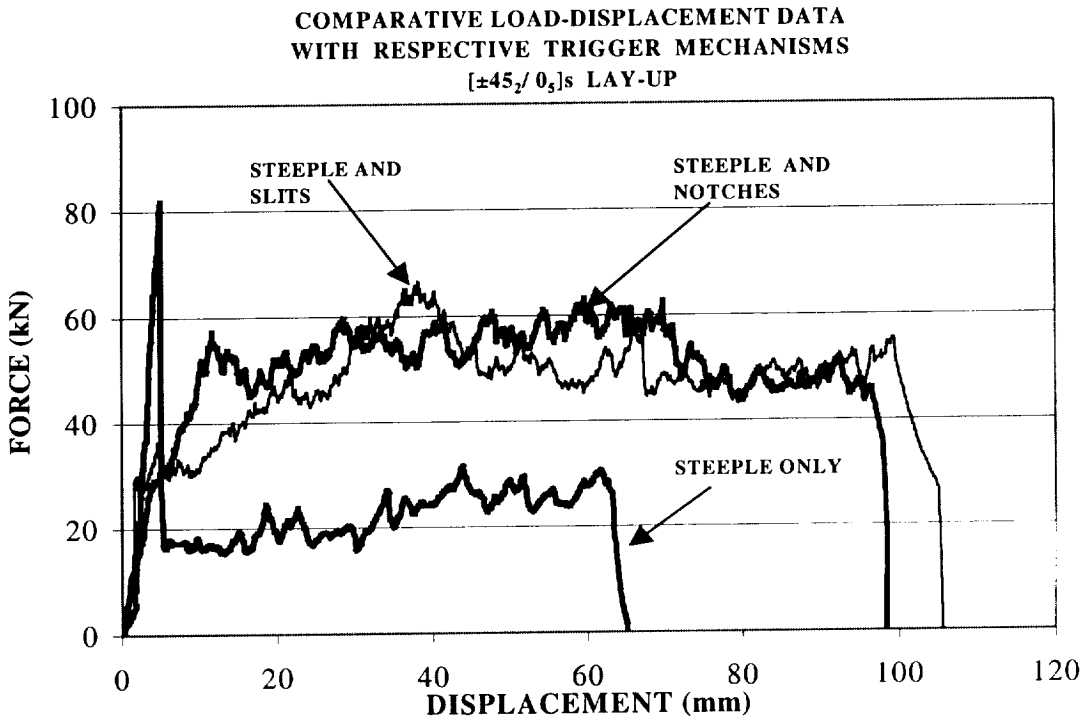

Figure 5 Comparison of plate crushing response using steeple chamfer and modified triggers (from Reference X)

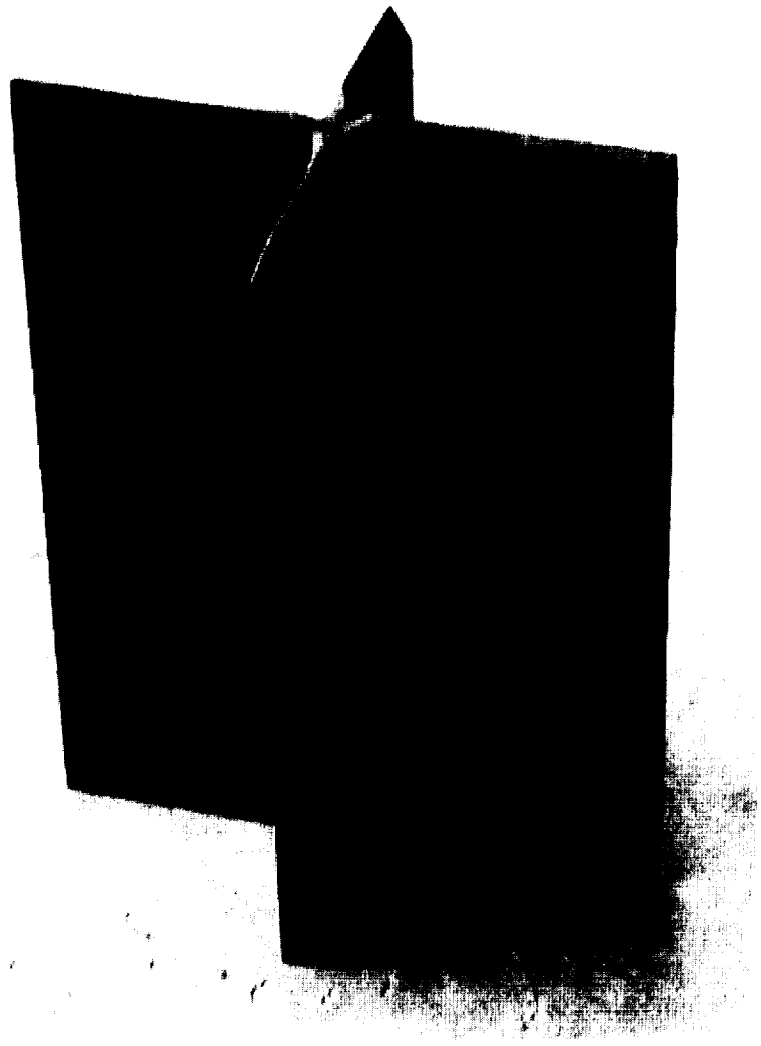

Figure 6 Typical x-column crushing specimen

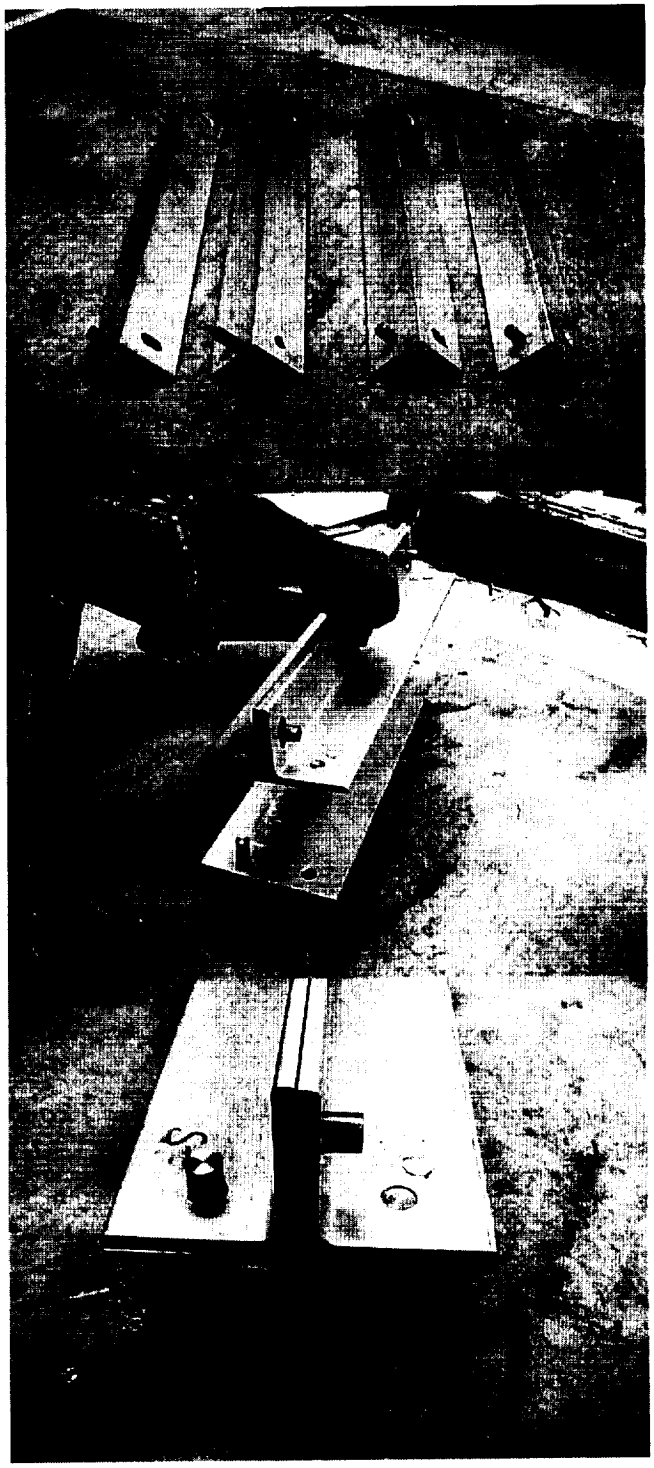

Figure 7 Aluminum mold used for the production of X-Column specimens

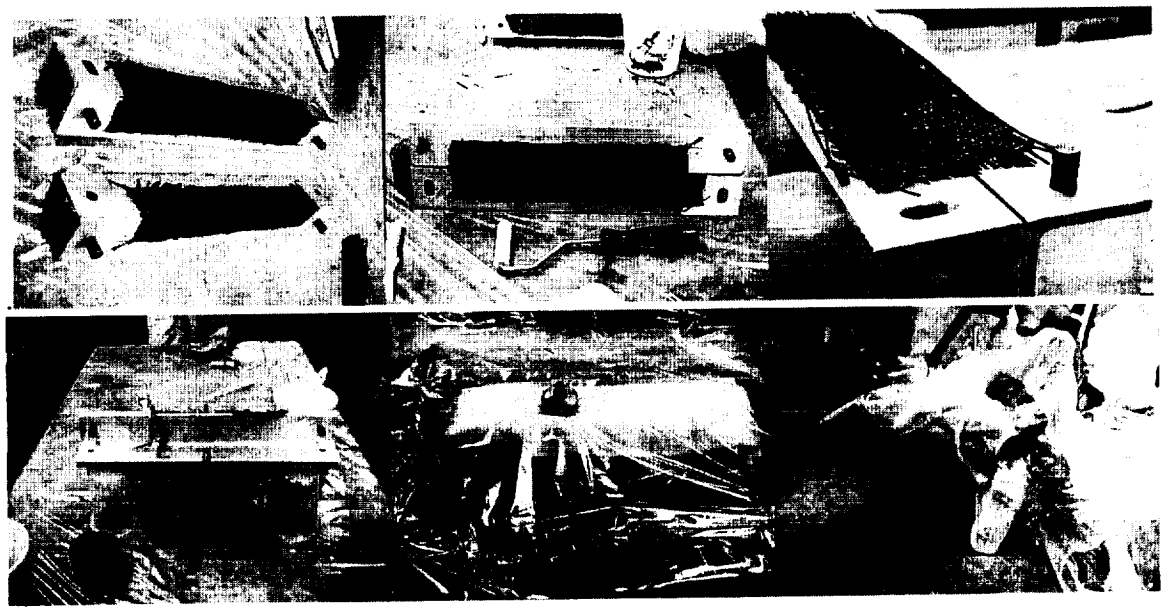

Figure 8 Lay-up and vacuum bagging procedure for X-column specimens

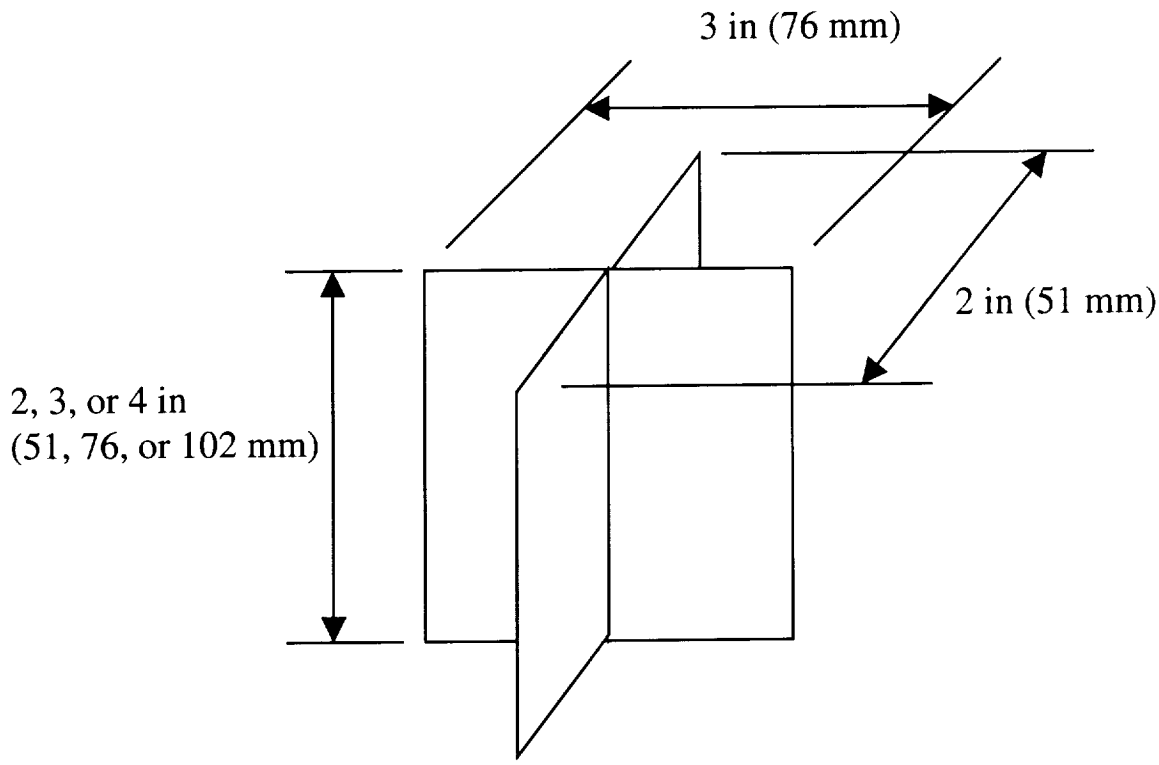

Figure 9 Nominal dimensions for X-Column specimens

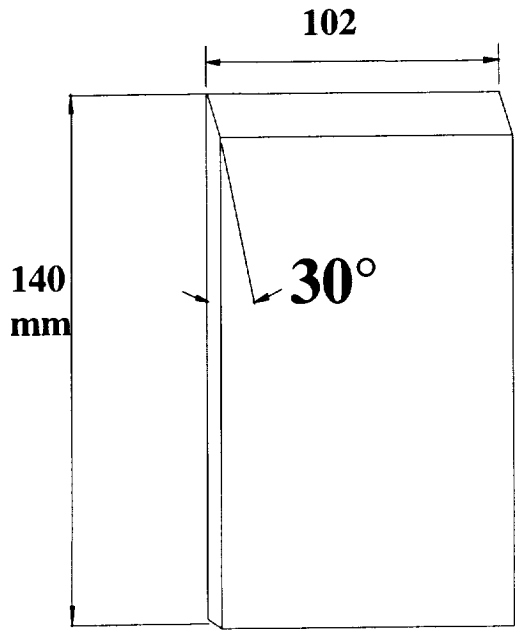

Figure 10 Plain chamfer crushing trigger

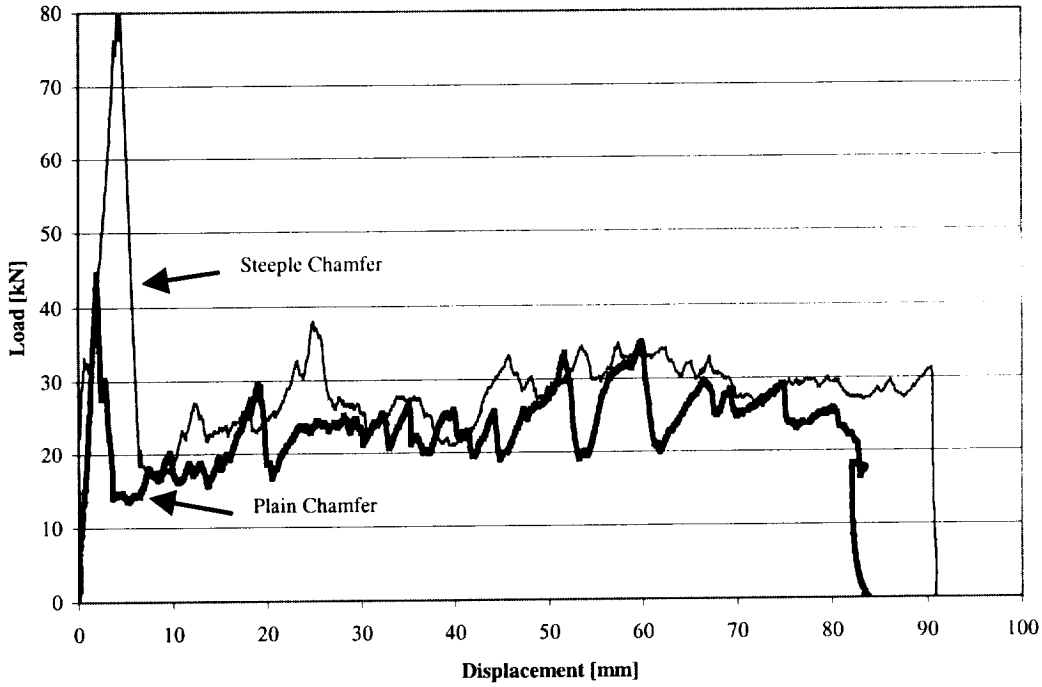

Figure 11 Comparison of plate crush test results for plain and steeple chamfer for a $[(\pm 45)_3/0_3]_S$ specimen

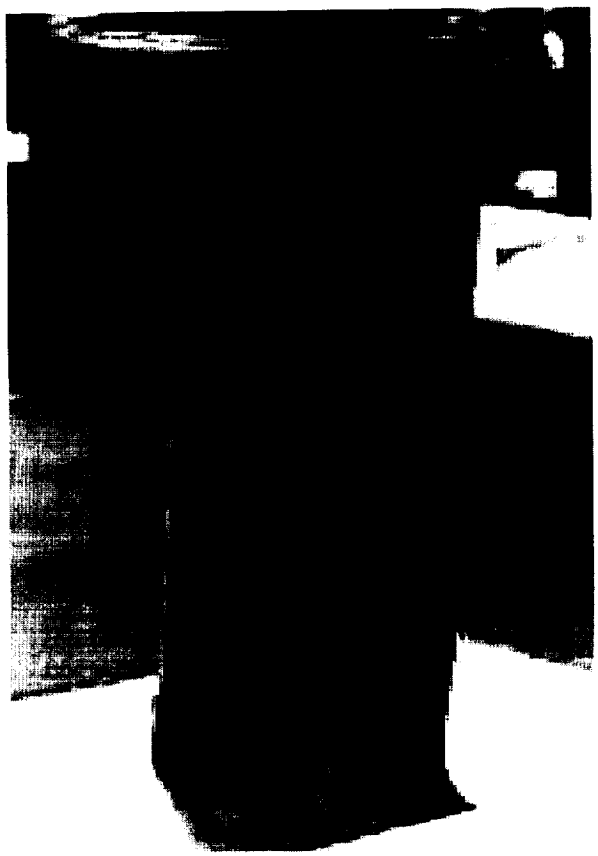

Figure 12 Instability in specimen X1-1 shortly after triggering

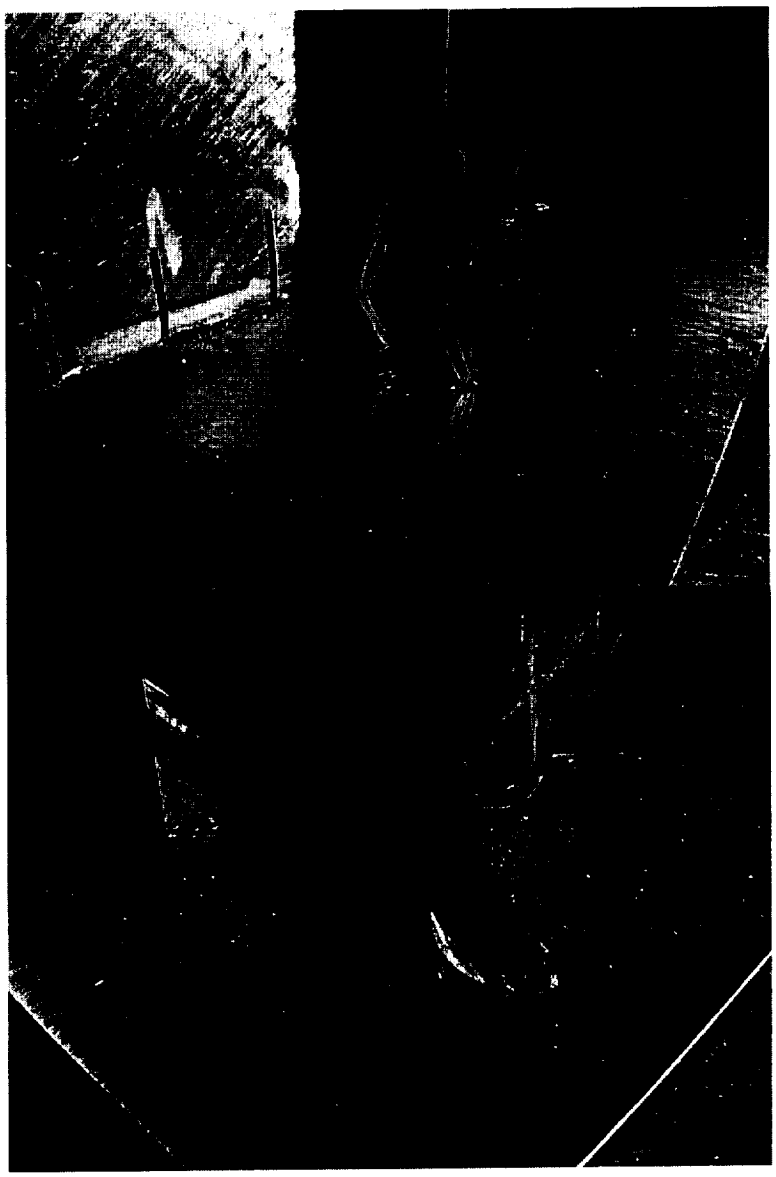

Figure 13 Triggering in specimen with chamfer + notches crushing trigger

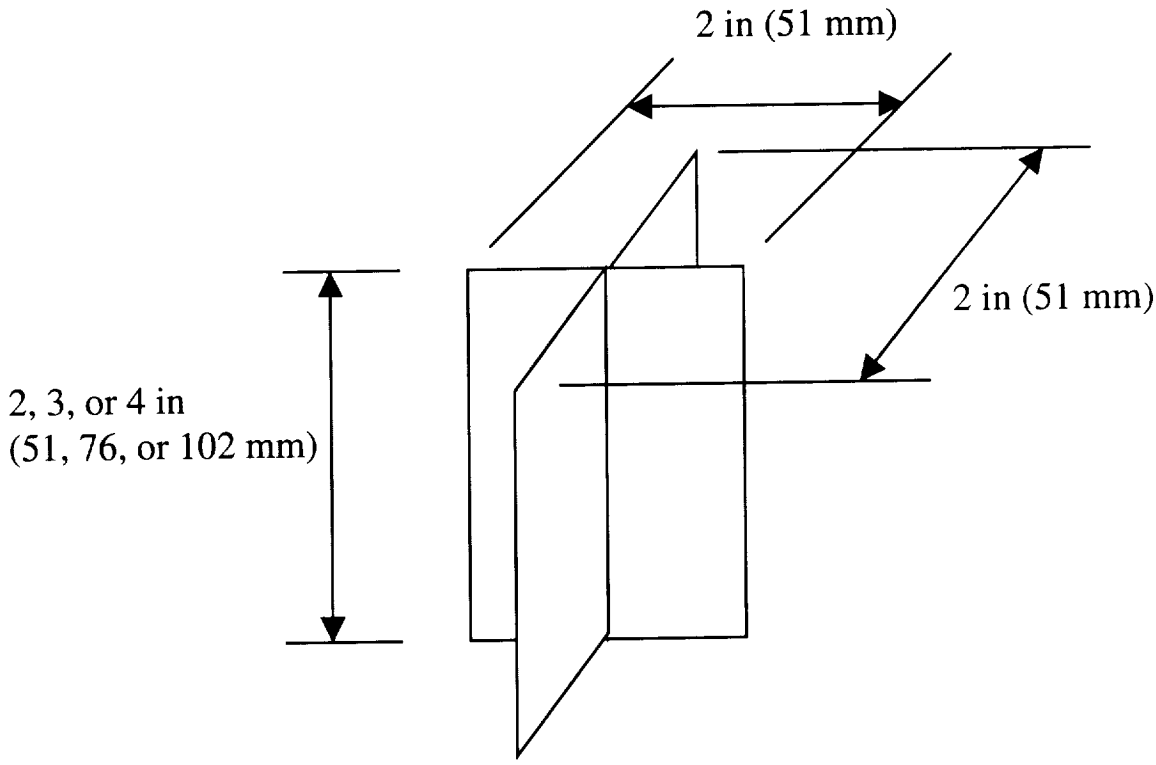

Figure 14 Nominal dimensions for reduced size X-Column specimens

Figure 15 Photographs from testing of specimen X1-3

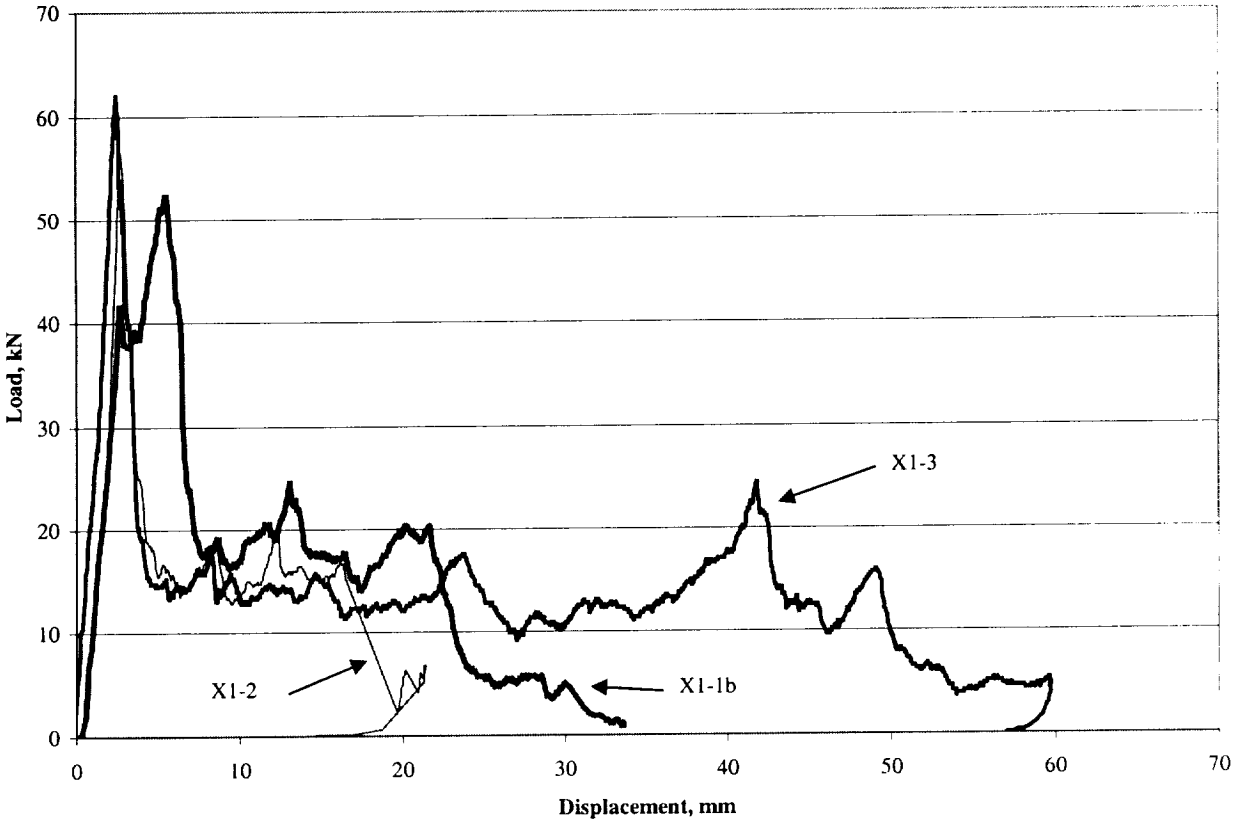

Figure 16 Load-displacement response for X-column specimens with a $[\pm 45_3/0_3]_S$ lay-up

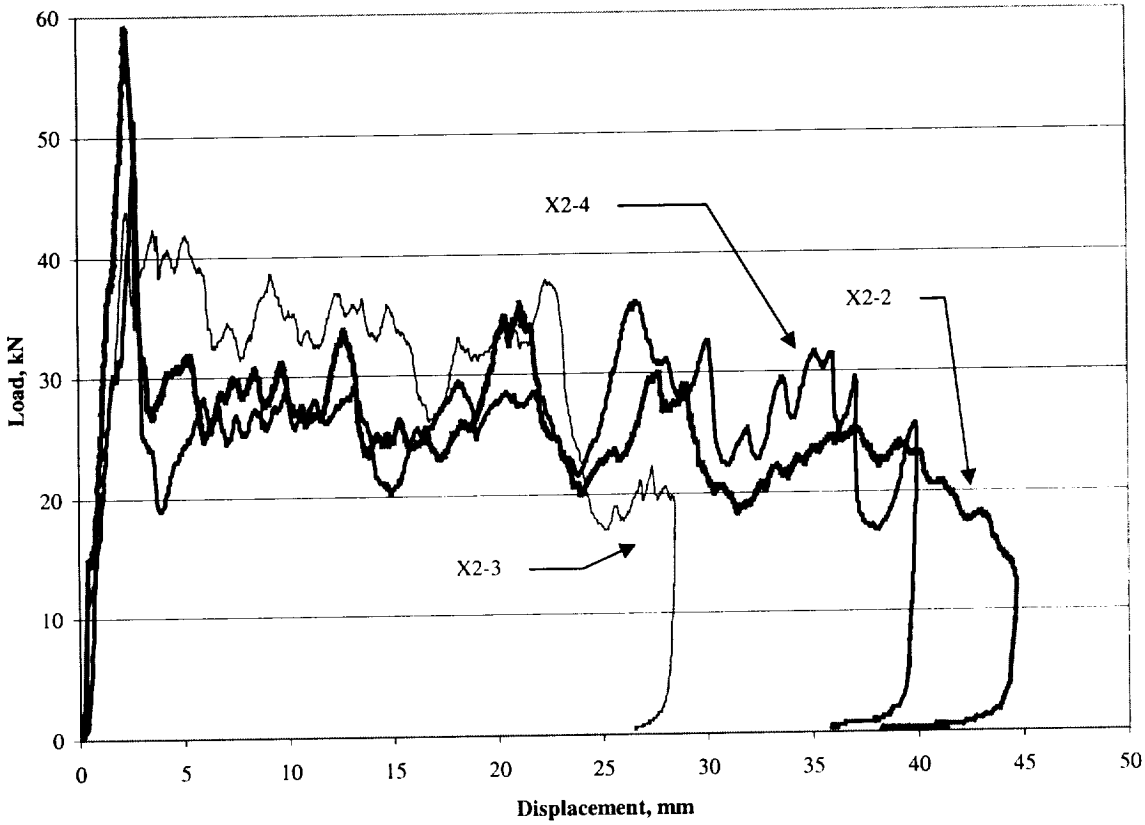

Figure 17 Load-displacement response for X-column specimens with a $[(\pm 45/0)_3]_S$ lay-up

Figure 18 Crushing of specimen X2-3 showing relatively low levels of damage in the deofrmed fronds.

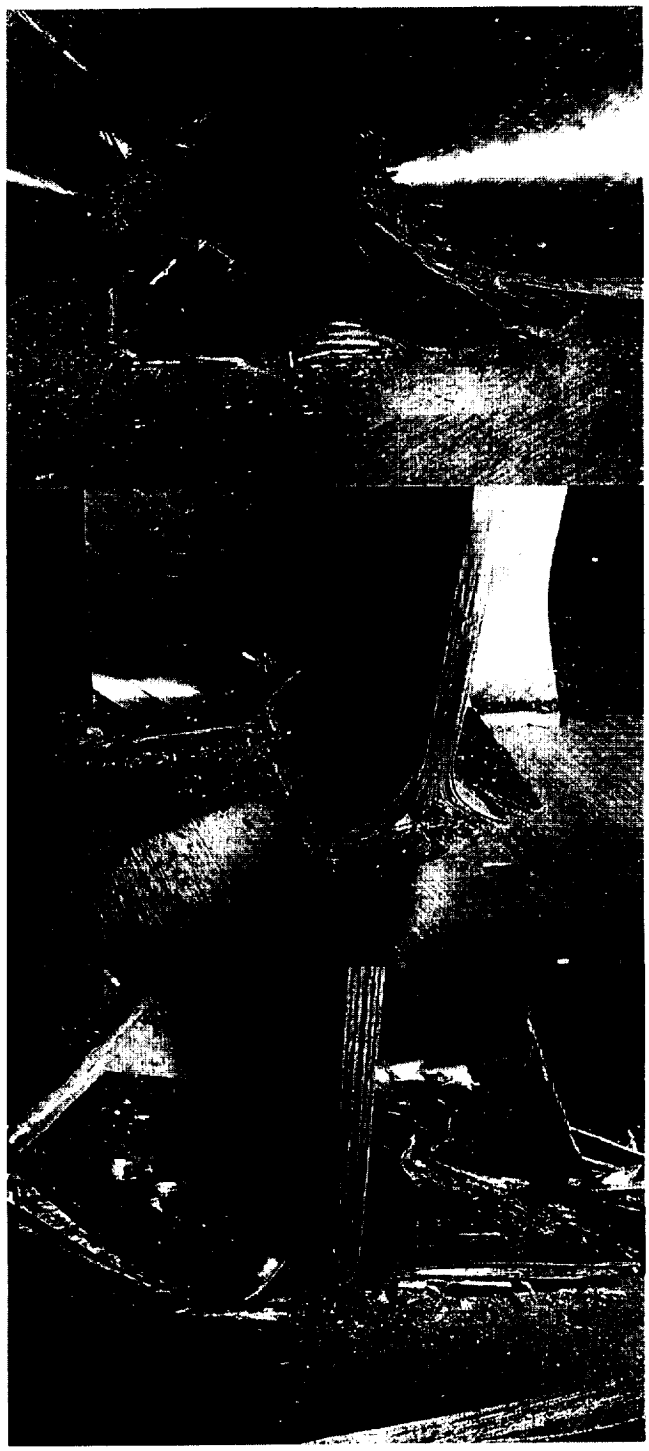

Figure 19 Detail of crushing from specimens X2-2, X2-3, and X2-4, respectively, showing localized damage in the central portion of the laminate

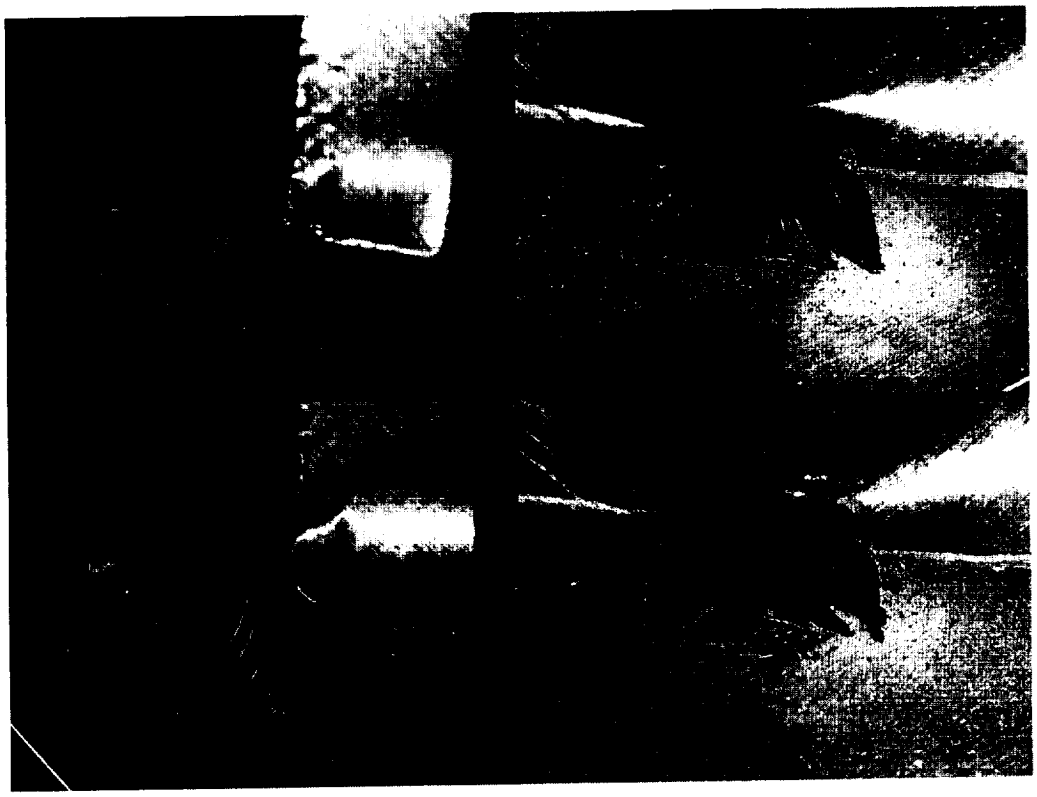

Figure 20 Damage state in each of the four arms of specimen X2-2 at approximately the same crushing displacement (the two longer arms are shown on the left and the two shorter arms on the right)

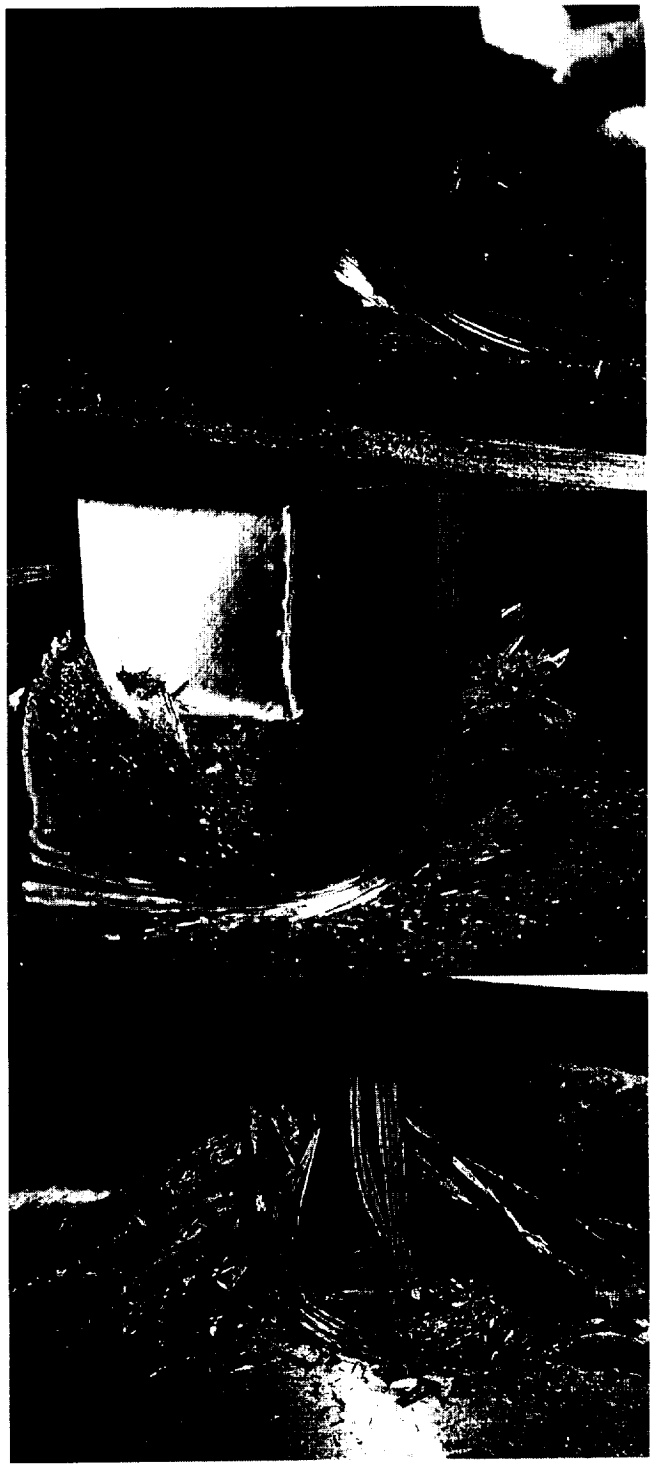

Figure 21 Through-thickness collapse of laminates in specimens X1, X2, and X4, respectively

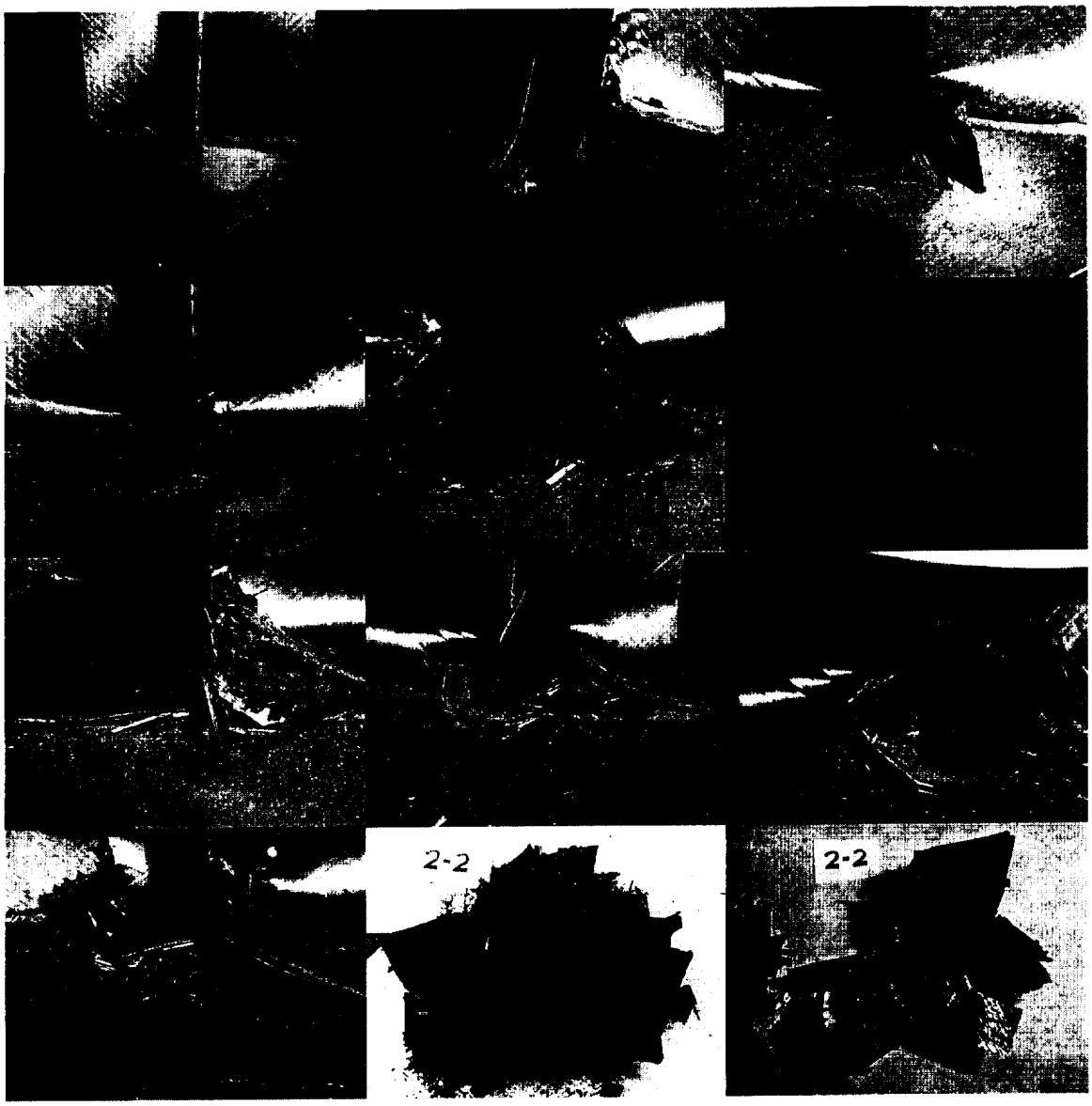

Figure 22 Crushing of specimen X2-2 (Note that different portions of the specimen are represented in the various photographs)

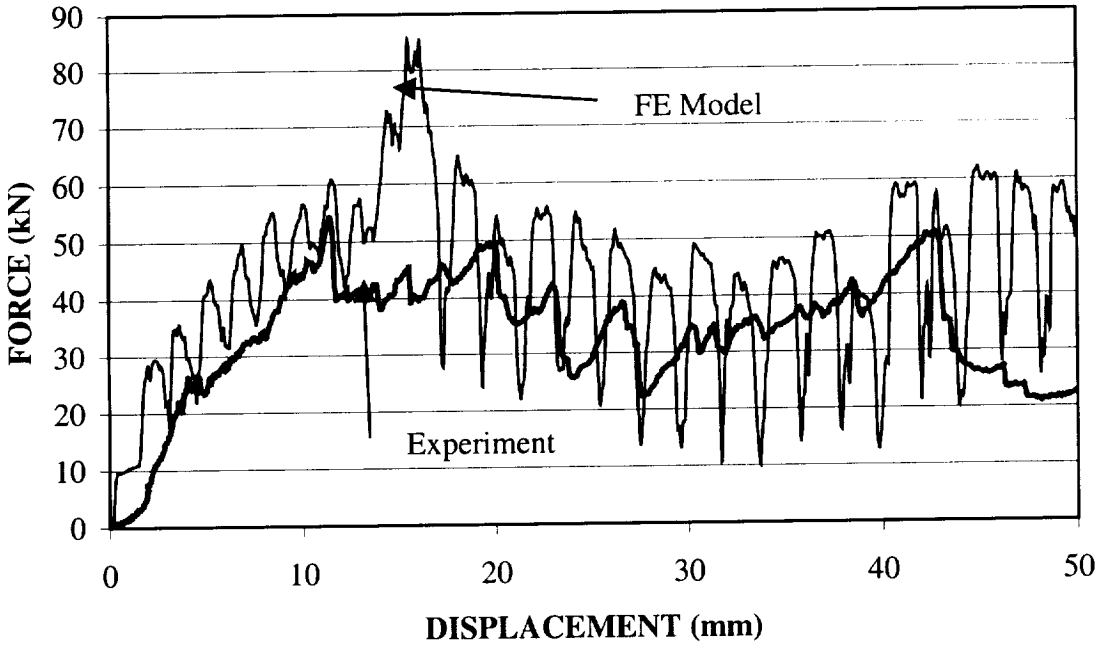

Figure 23 Comparison of LS-DYNA and experimental results for a $[(\pm 45)_3/0_3]_S$ plate [28]

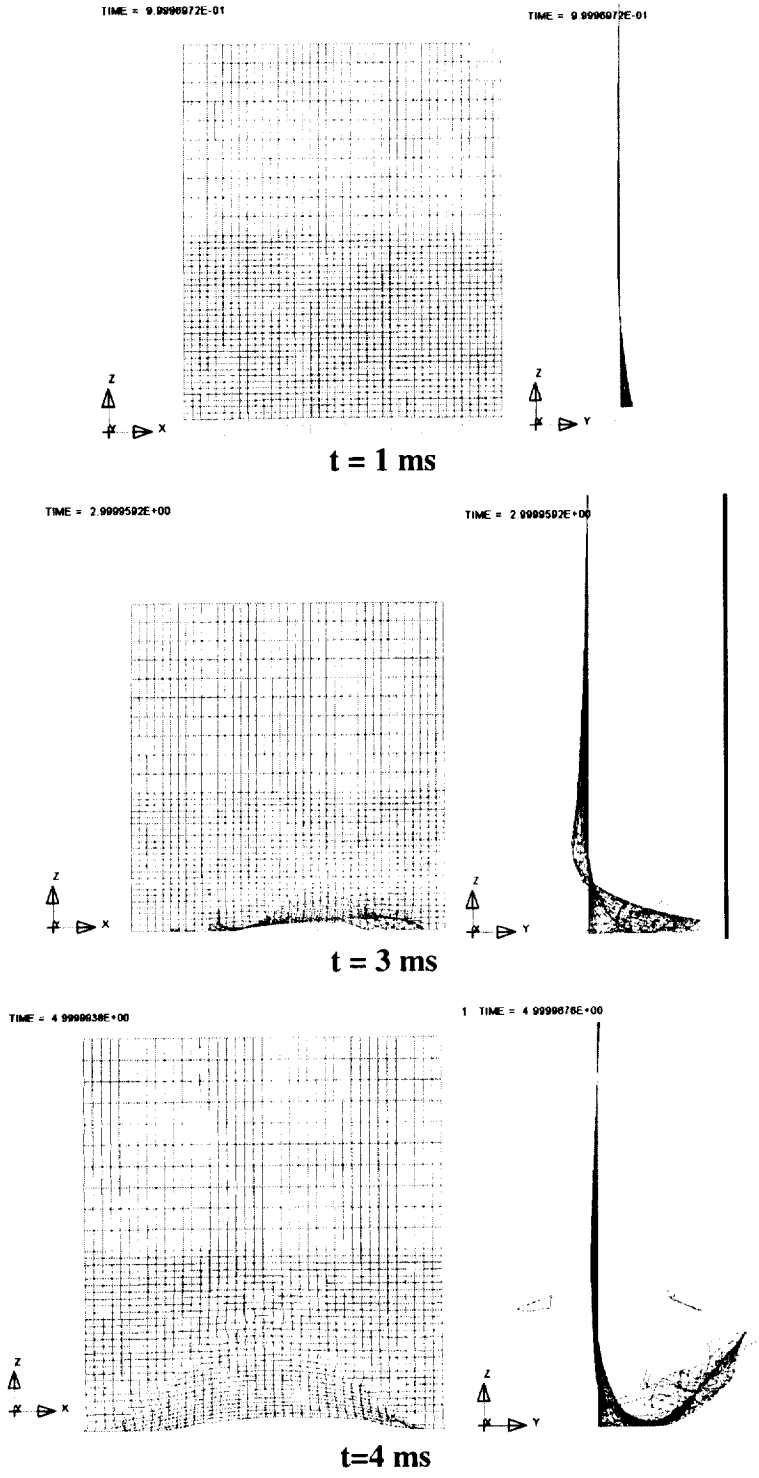

Figure 24 Deformation shapes for LS-DYNA model of plate crushing of a $[(\pm 45)_3/0_3]_S$ lay-up specimen

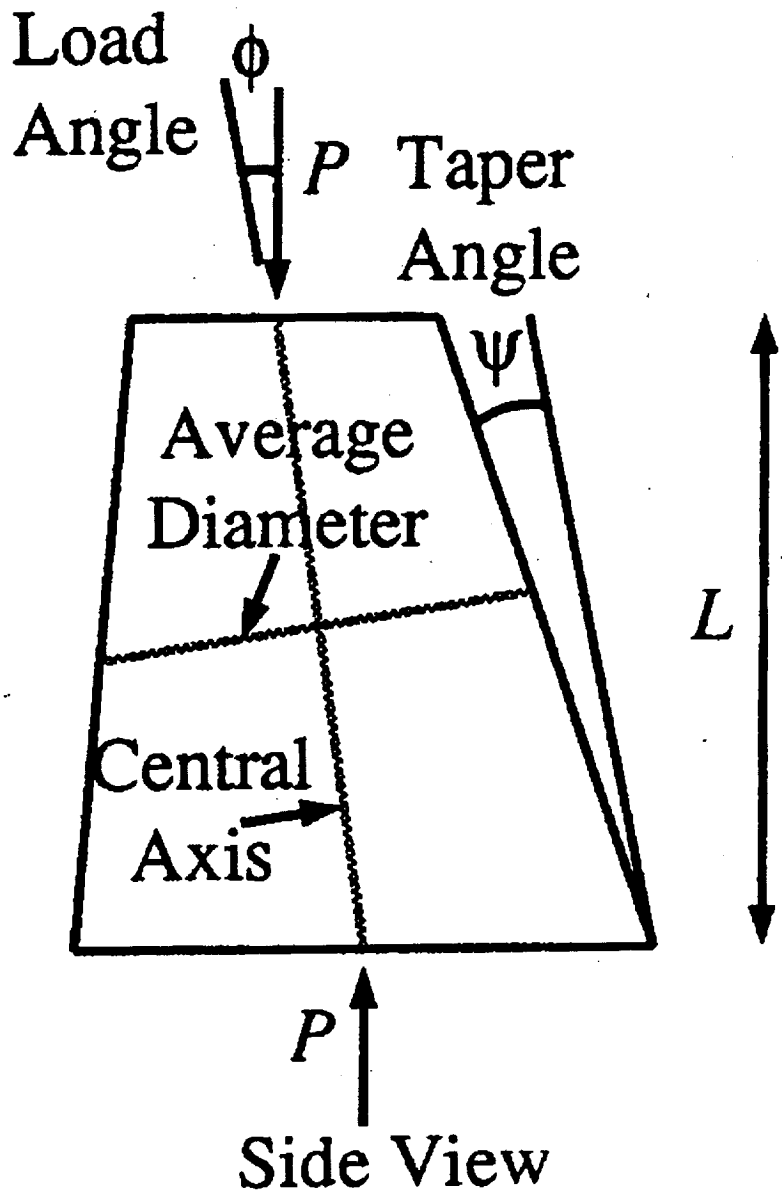

Figure 25 Truncated cone crushing specimen geometry (from Reference 35)

Figure 26 Crushing sequence of graphite/epoxy truncated cone (1° taper, 5° loading angle)

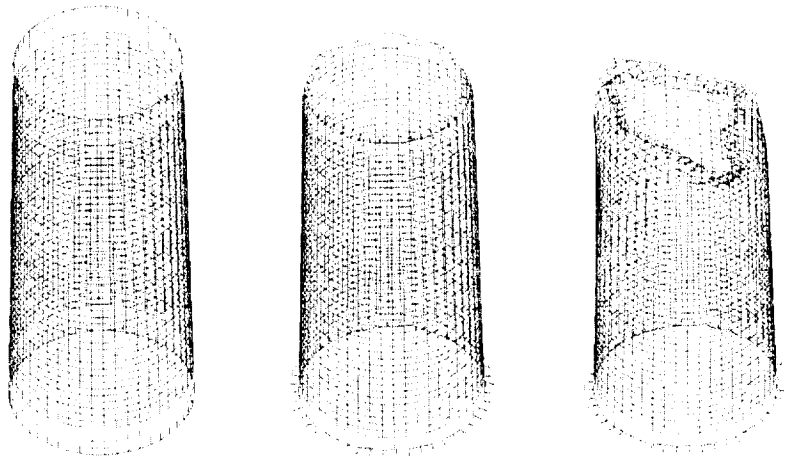

Figure 27 Deformed shapes of truncated cone specimens loaded by planes offset by 5° to the cone axis modeled using LS-DYNA Material 55 (enhanced composite damaging model)

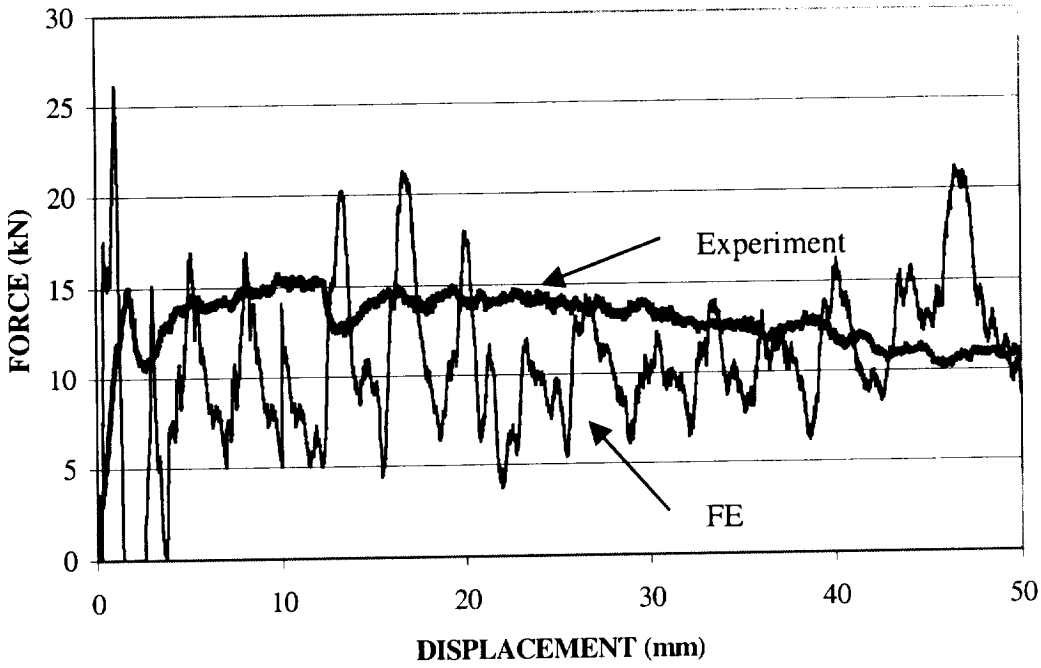

Figure 28 Comparison between finite element and experimental results for a truncated cone with 1° taper and 0° cut angle [28]

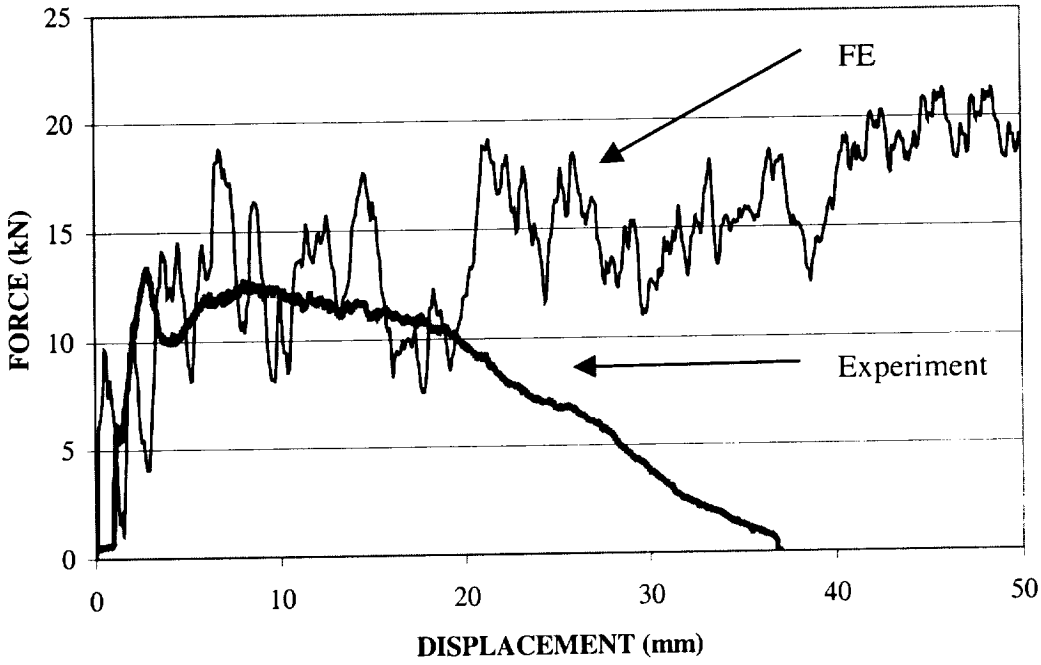

Figure 29 Comparison between finite element and experimental results for a truncated cone with 1° taper and 5° cut angle [28]

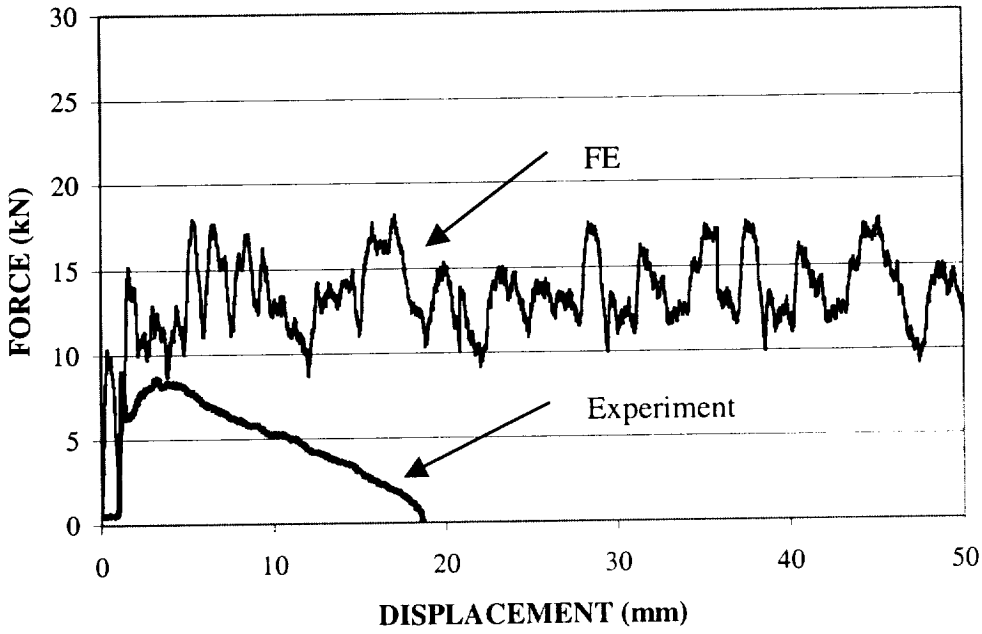

Figure 30 Comparison between finite element and experimental results for a truncated cone with 1° taper and 10° cut angle [28]

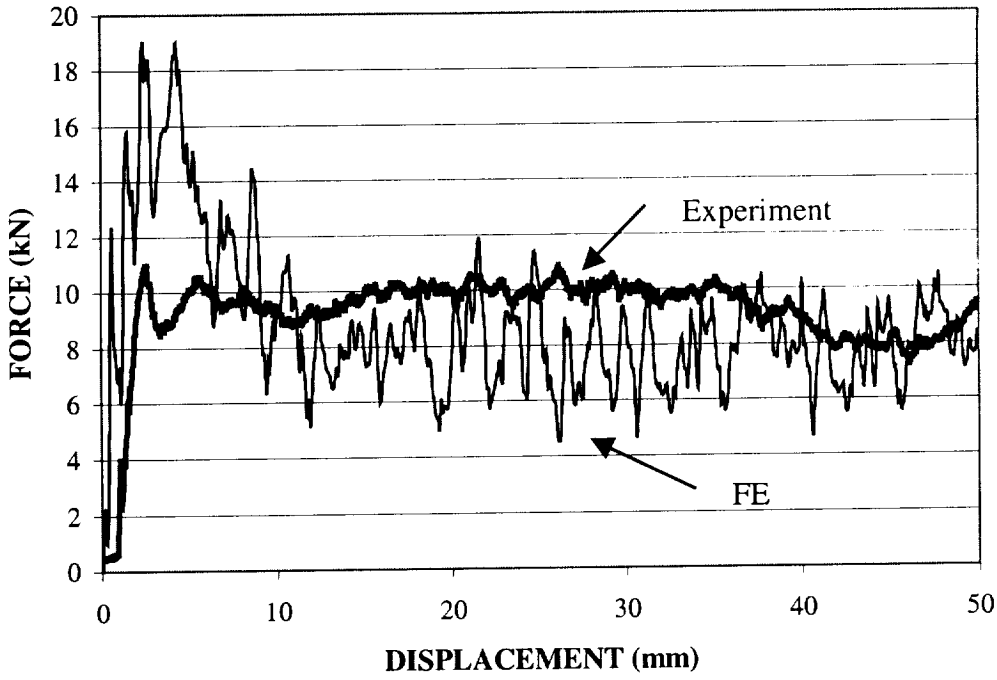

Figure 31 Comparison between finite element and experimental results for a truncated cone with 5° taper and 5° cut angle [28]

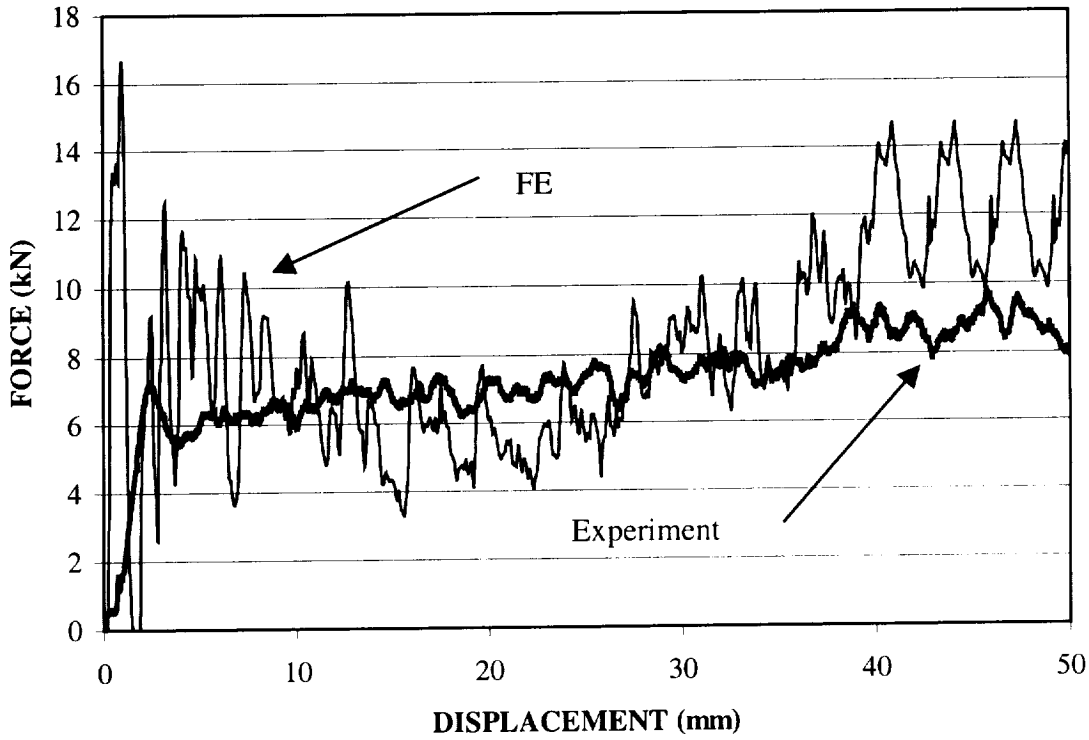

Figure 32 Comparison between finite element and experimental results for a truncated cone with 10° taper and 5° cut angle [28]

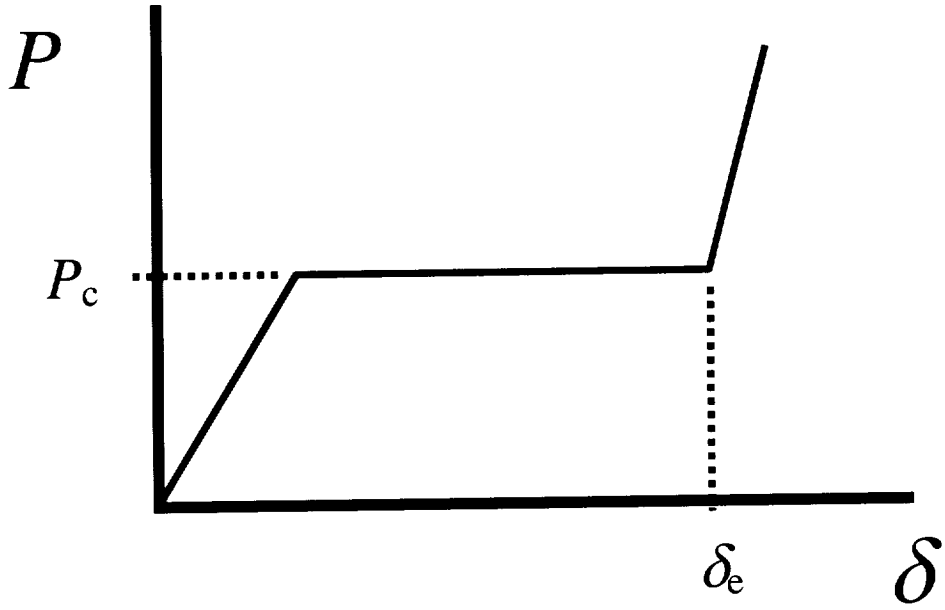

Figure 33 Idealized force-displacement curve

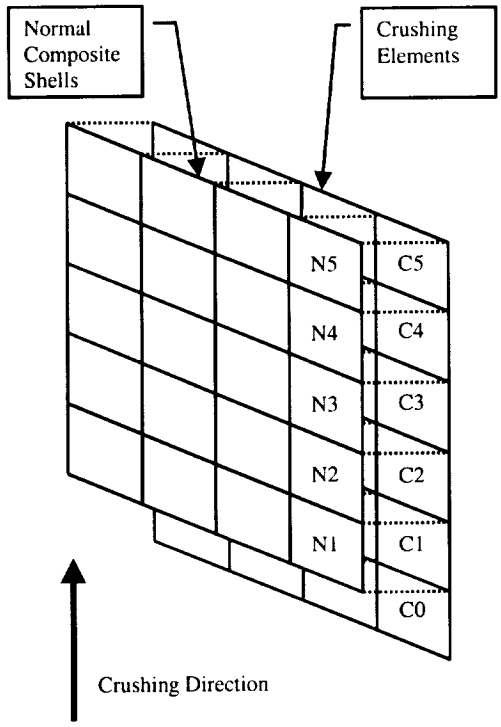

(a)

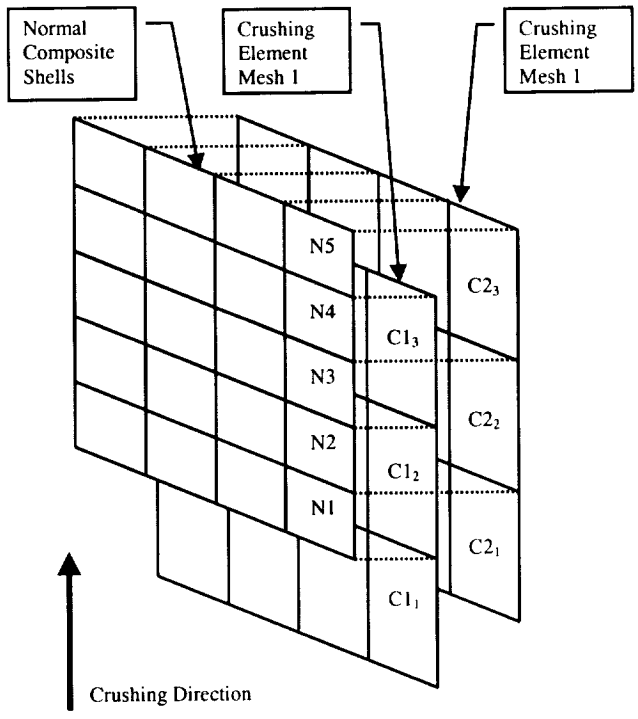

(b)

Figure 34 Schematic drawing of crushing mesh concept (a) basic configuration (b) with offset crushing meshes

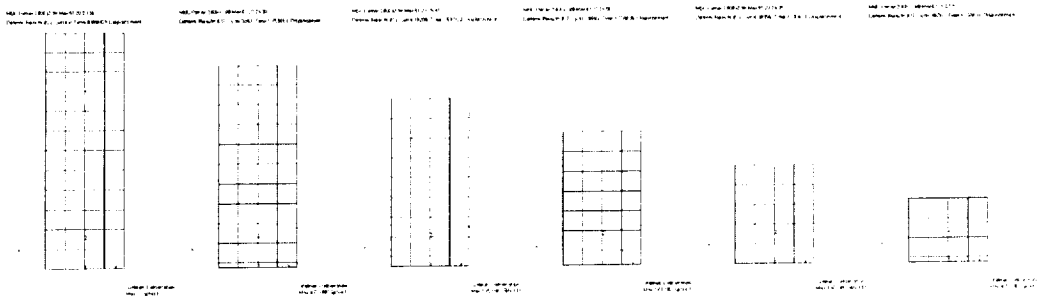

Figure 35 Deformation sequence for a rectangular plate showing progressive crushing damage

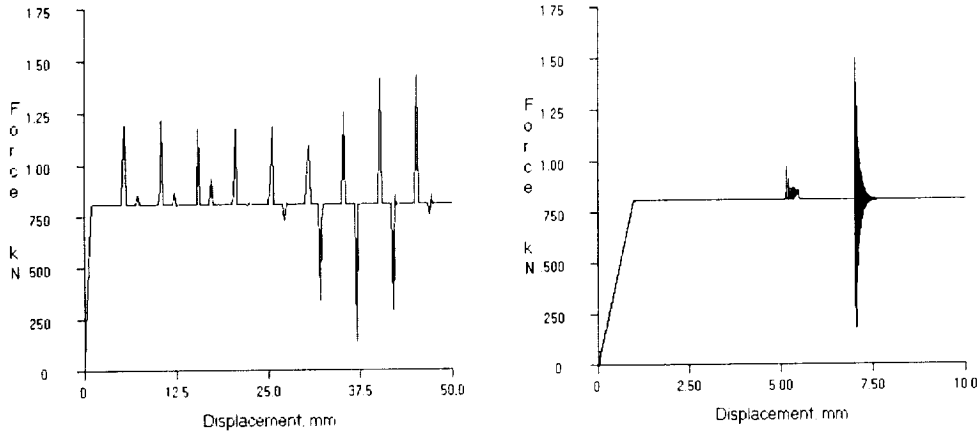

(a) (b)

Figure 36 Force versus time response for the rectangular plate model (a) complete crushing (b) highlighting the first handoff

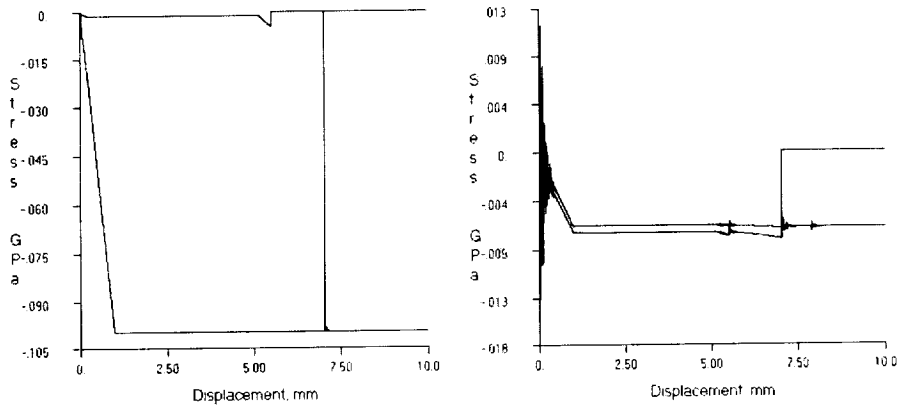

(a) **(b)**

Figure 37 Stress in the crushing direction during the first handoff (a) crushing elements $C1_1$ and $C2_1$ (b) composite elements N1 and N2

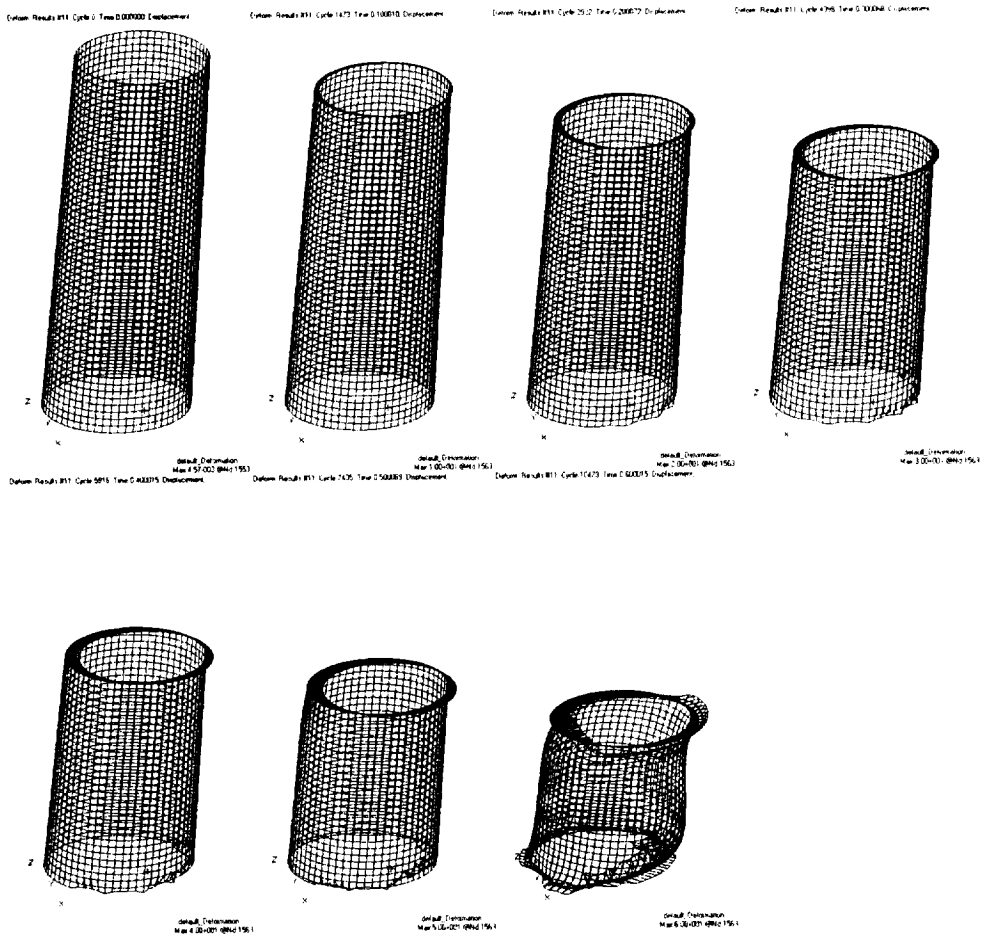

Figure 38 Displacement sequence for a model of a 1° taper, 5° cut truncated cone crushing specimen

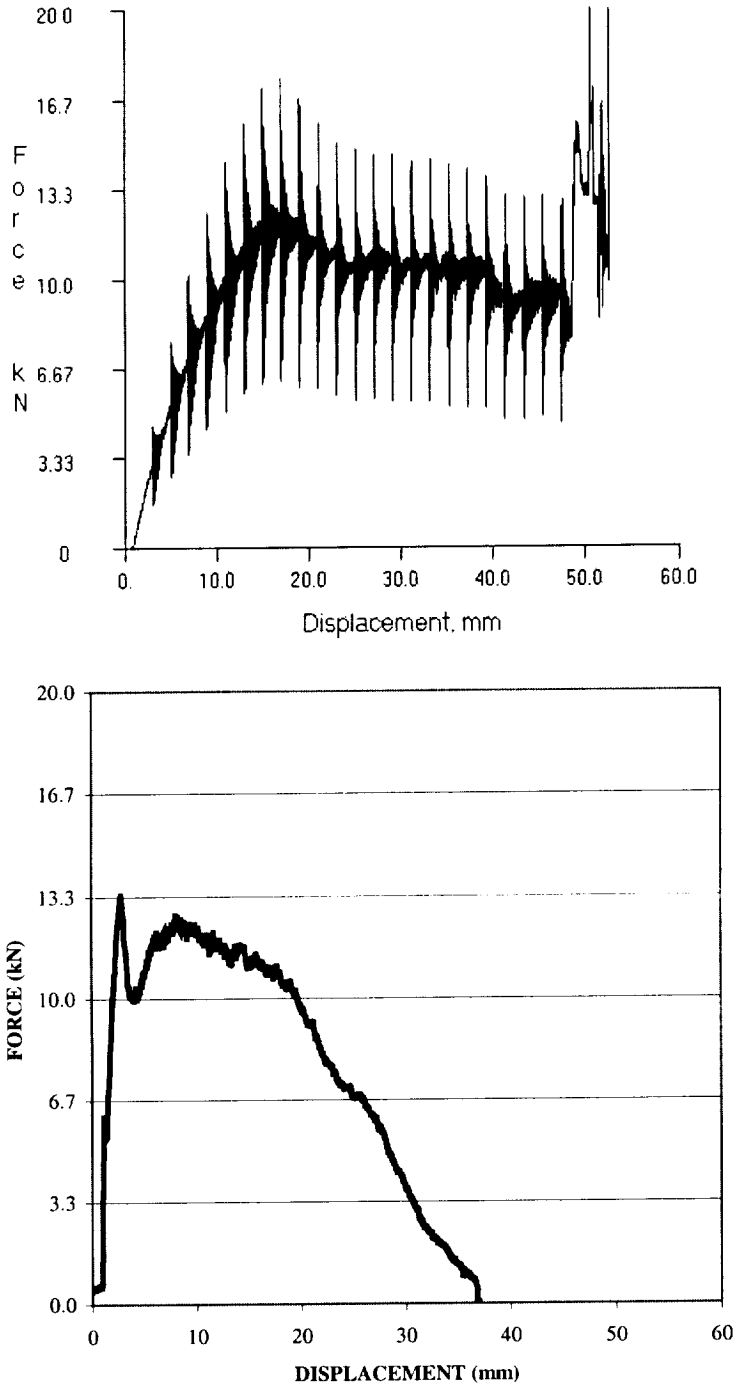

Figure 39 Force versus displacement response for a 1° taper, 5° cut truncated cone crushing specimen from Dytran crushing model (top) and experimental result (bottom)

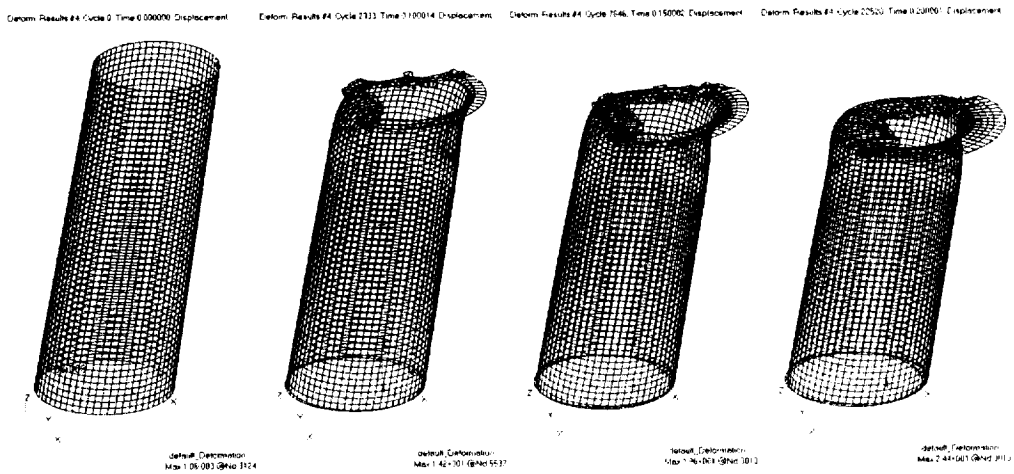

Figure 40 Displacement sequence for a model of a 1° taper, 10° cut truncated cone crushing specimen